Molecular Distances from Dipolar Coupled Spin-Labels: The Global Analysis of Multifrequency Continuous Wave Electron Paramagnetic Resonance Data

Eric J. Hustedt,* Alex I. Smirnov,# Charles F. Laub,* Charles E. Cobb,* and Albert H. Beth*
*Department of Molecular Physiology and Biophysics, Vanderbilt University, Nashville, Tennessee 37232, and #Illinois EPR Research Center, University of Illinois at Urbana, Urbana, Illinois 61801 USA

ABSTRACT For immobilized nitroxide spin-labels with a well-defined interprobe geometry, resolved dipolar splittings can be observed in continuous wave electron paramagnetic resonance (CW-EPR) spectra for interelectron distances as large as 30 Å using perdeuterated probes. In this work, algorithms are developed for calculating CW-EPR spectra of immobilized, dipolar coupled nitroxides, and then used to define the limits of sensitivity to the interelectron distance as a function of geometry and microwave frequency. Secondly, the CW-EPR spectra of N^6-spin-labeled coenzyme NAD^+ bound to microcrystalline, tetrameric glyceraldehyde-3-phosphate dehydrogenase (GAPDH) have been collected at 9.8, 34, and 94 GHz. These data have been analyzed, using a combination of simulated annealing and global analysis, to obtain a unique fit to the data. The values of the internitroxide distance and the five angles defining the relative orientation of the two nitroxides are in reasonable agreement with a molecular model built from the known crystal structure. Finally, the effect of rigid body isotropic rotational diffusion on the CW-EPR spectra of dipolar coupled nitroxides has been investigated using an algorithm based on Brownian dynamics trajectories. These calculations demonstrate the sensitivity of CW-EPR spectra to dipolar coupling in the presence of rigid body rotational diffusion.

INTRODUCTION

Nitroxide spin-labels have been used with great success in a number of recent studies to determine structural features of soluble and membrane-bound proteins (Hubbell and Altenbach, 1994; Hubbell et al., 1996; Millhauser, 1992). An emerging general method, called site-directed spin-labeling, takes advantage of the power of molecular biological approaches to introduce unique labeling sites into proteins of interest through site-directed mutagenesis. These sites, usually cysteine residues, are then covalently reacted with nitroxide spin-labeling reagents, which have high specificity for the thiol side-chain of cysteine. Hubbell and coworkers have developed a strategy for determining the structural environment near the labeled residue through straightforward analysis of the continuous wave electron paramagnetic resonance (CW-EPR) lineshape and through measurement of the accessibility of the labeled side chain to various paramagnetic broadening agents. By constructing a series of single cysteine mutants, elements of secondary, tertiary, and quaternary structure of both soluble and membrane-bound proteins can be mapped using this approach. A number of proteins have been investigated using site-directed spin-labeling including bacteriorhodopsin (Altenbach et al., 1990), rhodopsin (Farahbakhsh et al., 1995), the transmembrane domain of diphtheria toxin (Oh et al., 1996), T4 lysozyme (Mchaourab et al., 1996), colicin E1 (Shin et al., 1993), Fep A receptor (Liu et al., 1994), lactose permease (Voss et al., 1996), and helical peptides (Miick et al., 1992), with more applications rapidly being developed in many laboratories. Recently, Millhauser and co-workers have synthesized helical peptides doubly labeled with a rigid spin-labeled glycine derivative, TOAC (Hanson et al., 1996a,b). Both exchange-coupled and dipolar-broadened spectra have been observed from these peptides.

An important aspect of site-directed spin-labeling is the development of methods for localizing elements of protein secondary structure relative to one another. One approach that has recently been used with some success is the measurement of the distance between two spin-labels via analysis of the dipolar coupling between the two probes (Hubbell et al., 1996). The measurement of molecular distances using the magnitude and characteristics of spin-spin interactions is well established in the scientific literature (Luckhurst, 1976; Eaton and Eaton, 1989). This method can be applied to protein structure determination if two nitroxides are site-specifically incorporated into a protein through any combination of site-directed spin-labeling and the binding of spin-labeled high-affinity ligands. Analytical methods have been developed for the determination of nitroxide-nitroxide distances from CW-EPR spectra of labeled proteins (Eaton and Eaton, 1989; Beth et al., 1984; Rabenstein and Shin, 1995). In addition, many previous applications have focused upon measuring distances between paramagnetic metals and nitroxide spin-labels (Eaton et al., 1983; Eaton and Eaton, 1989; Voss et al., 1995a,b). Finally, a number of groups have developed time-domain EPR techniques suitable for the measurement of electron spin-spin distances in solid samples (Pfannebecker et al., 1996; Sax-

Received for publication 18 October 1996 and in final form 10 January 1997.

Address reprint requests to Dr. Albert H. Beth, Department of Molecular Physiology and Biophysics, 727 Light Hall, Vanderbilt University, Nashville, TN 37232-0615. Tel.: 615-322-4235; Fax: 615-322-7236; E-mail: beth@lhmrba.hh.vanderbilt.edu.

0006-3495/97/04/1861/17 $2.00

ena and Freed, 1996; Rakowsky et al., 1995; Larsen and Singel, 1993; Raitsimring et al., 1992).

In general terms, the determination of molecular distances from spin-spin interactions between nitroxide spin-labels requires consideration of the effects of dipolar and exchange coupling between the interacting spins. Appropriate computational algorithms have been developed for immobilized spins related by a well-defined geometry (Eaton et al., 1983). These algorithms have been previously used to estimate interprobe distance and geometry in spin-labeled proteins (Beth et al., 1984). However, the unique determination of all of the independent variables relating the dipolar coupled probes (one distance and five angles) has remained a formidable problem. In addition, the effect of the modulation of the relative orientations and distances between the spins due to local structural fluctuations and independent spin-label mobility, and the global rotational motion of the molecule, have not been considered. Despite the fact that elegant theoretical work has addressed the effects of local and global dynamics on spatially isolated nitroxide spin-labels (Freed, 1976; Dalton, 1985; Schneider and Freed, 1989), there has been little effort to extend these computational models to dipolar coupled spin-labels.

In the present work, three separate issues regarding the analysis of CW-EPR data from dipolar coupled nitroxide spin-labels have been addressed. First, a computationally efficient algorithm has been developed for calculating the CW-EPR spectrum of dipolar coupled nitroxides in the rigid limit. Using this algorithm, the sensitivity of CW-EPR spectra to the interelectron distance and the geometry relating the two nitroxides has been explored. These studies provide a guide to understanding the origins of various spectral features from dipolar coupled spin-labels and to predicting the sensitivity to interelectron separation as a function of microwave frequency.

Secondly, glyceraldehyde-3-phosphate dehydrogenase (GAPDH), a tetrameric protein with known crystal structure (Mercer et al., 1976; Moras et al., 1975) has been studied using an N^6-spin-labeled derivative of the coenzyme NAD (N^6-SL-NAD^+) by CW-EPR spectroscopy at 9.8, 34, and 94 GHz. In previous studies it has been shown that in the fully labeled tetramer there is a strong dipolar coupling between the two pairs of spin-labeled cofactors related by the crystallographic R axis and that X-band EPR data are consistent with an *anti-anti* conformation of N^6-SL-NAD^+ (Deparade et al., 1981; Beth et al., 1984). In the present work, it is shown that a unique assignment of the geometry between interacting, R axis-related spin-labels and their distance of separation can be obtained without any prior knowledge of the holoenzyme structure. These geometry and distance results have then been compared to a molecular model of the N^6-SL-NAD^+-GAPDH complex constructed based upon the known crystal structure. The results of this comparison indicate that the parameters obtained from fitting the EPR data are consistent with a structure in which the NAD^+ backbone of N^6-SL-NAD^+ is in the same position as natural NAD^+ and the spin-label moiety occupies a pocket between amino acid side chains.

Finally, the effects of rigid body rotational diffusion on the lineshapes from dipolar coupled nitroxide spin-labels are examined assuming axially symmetric A- and g-tensors and assuming that the interelectron vector is aligned with the nitroxide z axes. These calculations are performed by simulating a free induction decay signal using a Monte Carlo approach to model the rotational dynamics (Robinson et al., 1992). These studies provide an important initial look at the effect of global, rigid body rotational diffusion on the CW-EPR spectra of dipolar coupled nitroxides and a theoretical framework for including the effects of local probe motion on lineshapes in future work.

METHODS

Sample preparation

Rabbit skeletal muscle holo-GAPDH with an absorbance ratio of 1.05 (280/260 nm) was isolated and characterized as described in previous work (Beth et al., 1984). The [^{15}N,D_{17}]-N^6-SL-NAD^+ was a generous gift from Dr. Wolfgang Trommer of Universität Kaiserslautern (Park and Trommer 1989). Apo-GAPDH, with an absorbance ratio >1.9, was prepared by charcoal treatment as previously described (Beth et al., 1984). Two samples were prepared for spectral characterization. First, holo-GAPDH was dissolved in 5 mM sodium phosphate, pH 8.0, at a concentration of 5 mg/ml. [^{15}N,D_{17}]-N^6-SL-NAD^+ was added to this sample at a ratio of 0.5 mol spin-labeled cofactor/mol GAPDH tetramer. Second, apo-GAPDH was diluted to 5 mg/ml in 5 mM sodium phosphate, pH 8.0, and 5.0 mol spin-labeled cofactor was added per mol GAPDH tetramer. The two samples were incubated on ice for 10 min, then the N^6-SL-NAD^+-GAPDH samples were precipitated by dropwise addition of 10 vol saturated ammonium sulfate, pH 8.0, to a gently stirred solution of the enzyme. The microcrystalline enzyme was pelleted by centrifugation at 10,000 × g for 30 min and washed once to remove unbound spin-labeled cofactor with 10 vol saturated ammonium sulfate, pH 8.0, which had been previously temperature equilibrated on ice. The pelleted enzyme from this wash was resuspended in a small volume of saturated ammonium sulfate as a slurry for recording EPR data. Double integration of the EPR spectra obtained from these samples indicated spin concentrations of ~20 μM and 200 μM for the low and high labeling stoichiometries, respectively. Based upon the enzyme concentrations determined from the absorbance at 280 nm (ϵ = 1 cm^2/mg) of a redissolved aliquot from each sample, this corresponded to ~0.3 and 3.4 mol spin-labeled cofactor bound/mol tetramer. Therefore, the EPR spectrum of the first sample (low labeling stoichiometry) should be dominated by the EPR spectrum of a bound, spatially isolated component, while the EPR spectrum of the second sample (high labeling stoichiometry) should be dominated by the EPR spectrum of bound, pairwise dipolar coupled component with a small bound, spatially isolated component due to incomplete (fewer than four mol spin-labeled cofactor/mol tetramer) labeling.

All EPR spectra were obtained from samples of the ammonium sulfate-precipitated enzyme. This allowed the enzyme to be kept in a stable form so that spectra at three different microwave frequencies could be obtained from the same sample. Previous work has shown that at X-band, the EPR spectra of soluble and ammonium sulfate-precipitated forms of the SL-NAD^+/GAPDH complex are essentially identical (Beth et al., 1984).

EPR spectroscopy

The CW-EPR spectra were recorded at 9.8 and 34 GHz on a Bruker (Billerica, MA) ESP-300 spectrometer with the sample temperature regulated at 4°C using the ER4110 variable temperature accessory. X-band (9.8 GHz) spectra were recorded in a standard TM_{110} cavity with samples

contained in a 50-μl glass capillary (Corning Glass Works, Corning, NY) using 100 kHz Zeeman field modulation of 0.25 Gauss amplitude (peak-to-peak) and a microwave observer field of 0.01 Gauss (peroxylamine disulfonate calibrated; Beth et al., 1983). Q-band (34 GHz) spectra were recorded in a TE_{011} cavity with the sample contained in a 0.3-mm i.d. quartz capillary (Vitro Dynamics Inc., Rockaway, NJ). Zeeman field modulation at 100 kHz frequency of 0.25 Gauss amplitude and a microwave observer field of 0.01 Gauss were used (peroxylamine disulfonate calibrated; Beth et al., 1983). W-band (94 GHz) spectra were recorded at the University of Illinois EPR research center on an instrument described previously (Smirnov et al., 1995; Wang et al., 1994) using a 1.0 Gauss modulation amplitude in a TE_{012} cavity with the sample contained in a 0.15-mm i.d. quartz capillary (Vitro Dynamics Inc., Rockaway, NJ).

Calculation of EPR spectra of dipolar coupled nitroxides in the rigid limit

The Hamiltonian describing the dipolar interaction between two nitroxides, including the electron Zeeman interactions, nitroxide nitrogen nuclear Zeeman interactions, the electron-nitrogen hyperfine interactions, and neglecting all nonsecular terms, is given in frequency units by

$$\begin{aligned}\hat{H} = {} & g_{zz}^{1\prime}\beta_e H_0 S_z^1 + g_{zz}^{2\prime}\beta_e H_0 S_z^2 - \omega_n(I_z^1 + I_z^2) \\ & + A_{xz}^{1\prime} I_x^1 S_z^1 + A_{yz}^{1\prime} I_y^1 S_z^1 + A_{zz}^{1\prime} I_z^1 S_z^1 \\ & + A_{xz}^{2\prime} I_x^2 S_z^2 + A_{yz}^{2\prime} I_y^2 S_z^2 + A_{zz}^{2\prime} I_z^2 S_z^2 \\ & - \frac{D}{4} S_+^1 S_-^2 - \frac{D}{4} S_-^1 S_+^2 + D S_z^1 S_z^2\end{aligned} \tag{1}$$

where g_{zz}^j, A_{xz}^j, A_{yz}^j, and A_{zz}^j are the appropriate elements of the g- and hyperfine (A-) tensors for electron j, w_n is the nuclear Zeeman frequency, H_0 is the applied DC magnetic field, β_e is the Bohr magneton, and the unique element of the dipolar coupling tensor, D, is given by

$$D = \frac{\gamma_e^2 \hbar}{|R|^3}(1 - 3\cos^2\mu) \tag{2}$$

where w here μ is the angle between the DC magnetic field and the interelectron vector, $\vec{R}$.

The geometry of the problem is defined by three Euler angle transformations (see Fig. 1), $R_1(\gamma, \beta, \alpha)$, which orients the A- and g-tensors of nitroxide 2 with respect to nitroxide, 1, $R_2(0, \xi, \eta)$, which orients the interelectron vector $\vec{R}$ with respect to the axis frame defined by nitroxide 1, and $R_3(0, \theta, \phi)$ which orients the DC magnetic field, $\vec{H}_0$, with respect to the axis frame of nitroxide 1. The A-tensors for the two nitroxides at each orientation are given by

$$\begin{aligned}A^{1\prime} &= R_3 A^1 (R_3)^{-1} \\ A^{2\prime} &= R_3 R_1 A^2 (R_1)^{-1} (R_3)^{-1}\end{aligned} \tag{3}$$

where A^1 and A^2 are the diagonalized nitroxide hyperfine tensors. Similar equations apply to the g-tensors. Finally,

$$\cos\mu = (0\ 0\ 1) R_3 R_2^{-1} \begin{pmatrix}0\\0\\1\end{pmatrix} \tag{4}$$

As is discussed in further detail in Appendix A, approximate eigenvalues and eigenvectors for the Hamiltonian of Eq. 1 are found by setting $\omega_n = 0$ and by neglecting the mixing of states with different nuclear spin quantum numbers. A simple transformation converts the Hamiltonian into block 4 × 4 diagonal form. There are four allowed transitions, labeled l = 1 through 4, for each 4 × 4 block, k.

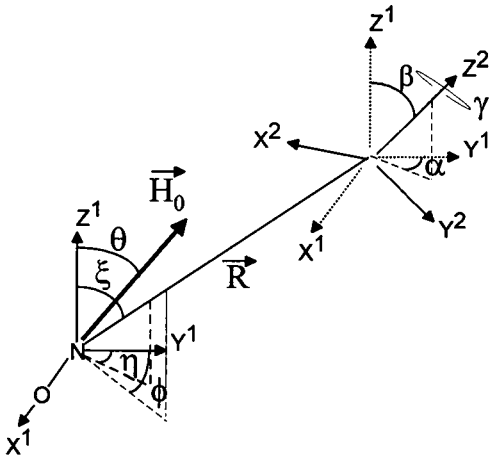

FIGURE 1 Diagram illustrating the two angles (ξ, η) relating the interelectron vector, $\vec{R}$, to the axis frame defined by nitroxide 1, and the three angles (α, β, γ) relating the orientation of nitroxide 2 to nitroxide 1. The angles θ and ϕ define the orientation of the external magnetic field, $\vec{H}$, with respect to the axis frame of nitroxide 1.

The applied magnetic field strength at which a particular transition is on resonance with the microwave frequency, ω_0, is given by (using l = 1 as an example),

$$\omega_0 - (\lambda_1^k - \lambda_2^k) = 0 \tag{5}$$

or based on the results of Appendix A,

$$H_{res}^{l=1,k} = \frac{\omega_0 - c^k - D/2 - \sqrt{(qH_{res}^{l=1,k} + f^k)^2 + (D/4)^2}}{p} \tag{6}$$

A reasonable estimate of $H_{res}^{l=1,k}$ can be obtained by approximating $H_{res}^{l=1,k}$ on the right-hand side of Eq. 6 by H_{CF}, the applied magnetic field at the center of the EPR spectrum.

$$(H_{res}^{l=1,k})' = \frac{\omega_0 - c^k - D/2 - \sqrt{(qH_{CF} + f^k)^2 + (D/4)^2}}{p} \tag{7}$$

This approximation of $H_{res}^{l=1,k}$ can then be used to obtain a more accurate estimate of the true value.

$$(H_{res}^{l=1,k})'' = \frac{\omega_0 - c^k - D/2 - \sqrt{(q(H_{res}^{l=1,k})' + f^k)^2 + (D/4)^2}}{p} \tag{8}$$

In practice, this procedure rapidly converges to give accurate values of the $H_{res}^{l=1,k}$.

The probabilities of the four allowed transitions are calculated at $H_0 = H_{res}^{l=1,k}$ as follows

$$\begin{aligned}P_{l=1,k} &= |\langle\Psi_1^k|S_+^1 + S_+^2|\Psi_2^k\rangle|^2 = (\nu_1^k - \nu_2^k)^2 \\ P_{l=2,k} &= |\langle\Psi_1^k|S_+^1 + S_+^2|\Psi_3^k\rangle|^2 = (\nu_1^k + \nu_2^k)^2 \\ P_{l=3,k} &= |\langle\Psi_2^k|S_+^1 + S_+^2|\Psi_4^k\rangle|^2 = (\nu_1^k - \nu_2^k)^2 \\ P_{l=4,k} &= |\langle\Psi_3^k|S_+^1 + S_+^2|\Psi_4^k\rangle|^2 = (\nu_1^k + \nu_2^k)^2\end{aligned} \tag{9}$$

where ν_1^k and ν_2^k are given in Appendix A.

The pair of nitroxides, rigidly oriented with respect to each other, are randomly oriented within the sample. The simulated CW-EPR spectrum is then given by the double integral, approximated by a double sum over the angles θ and ϕ.

$$S(H_0) = \sum_{l=1}^{4} \sum_{k} \sum_{m=1}^{N_\phi} \sum_{n=1}^{N_\theta} \frac{\sin \theta_n}{N_\theta N_\phi} \frac{P_{l,k}(H_0 - H_{res}^{l,k\prime\prime}(\theta_n, \phi_m))}{(\Gamma^2 + (H_0 - H_{res}^{l,k\prime\prime}(\theta_n, \phi_m)} \tag{10}$$

where

$$\Delta_\phi = \frac{2\pi}{N_\phi} \quad \phi_m = (m-1)\Delta_\phi$$
$$\Delta_\theta = \frac{\pi}{N_\theta} \quad \theta_n = \left(n - \frac{1}{2}\right)\Delta_\theta \tag{11}$$

and Γ is the Lorentzian linewidth. The simulation $S(H_0)$ is then convolved with a Gaussian broadening function of width, σ, to account for additional broadening due to couplings to protons or deuterons not included in the Hamiltonian of Eq. 1.

Nonlinear least-squares analysis

The EPR spectra of spatially isolated nitroxide spin-labels were fit to a powder pattern model using a nonlinear least-squares global analysis method as previously described (Hustedt et al., 1993). The algorithm developed in the previous section (Eq. 10) for the calculation of the CW-EPR spectra of dipolar coupled nitroxides was incorporated into this same global analysis program. The presence of multiple local minima in the multidimensional (one distance and five angles) χ^2 surface presented a significant difficulty in the analysis of spectra of dipolar coupled nitroxides using the Marquardt-Levenberg algorithm. Therefore, a program for the fitting of data to the dipolar coupled nitroxide model was developed based on the method of simulated annealing (Press et al., 1992). The simulated annealing minimization technique is well suited for exploring a surface with many local minima. In the present work, the simulated annealing program was used for fitting of single data sets (i.e., data obtained at a single microwave frequency).

Two approaches were taken to the simultaneous nonlinear least-squares analysis of the spectra of dipolar coupled nitroxides obtained at X-, Q-, and W-band. In the first method, a stepwise approach was used. Estimates of the interelectron distance were obtained from the observed splitting of the high field z-turning point assuming $\xi = 0°$ or $\xi = 90°$. Initially only the parameters R, ξ, and η were varied. Then the remaining angles (α, β, and γ) and the linewidths of the dipolar coupled components at the three microwave frequencies were varied to further refine the fit.

In the second method, the X-band spectrum was analyzed using the method of simulated annealing as described by Press et al. (1992). The algorithm was initialized with a random set of parameters (within physically reasonable limits) and run for 2000–4000 iterations, cooling at a rate given by $T_{n+1} = a\,T_n$, where a ranged from 0.95 to 0.999. At the end, the set of parameters that had given the smallest χ^2 was saved and used as a starting point for global analysis of all three data sets. Each trial solution could be obtained in ~5 h of computation time and a total of 10 such trial parameter sets were generated and used to initialize the global analysis.

In either case, the data was fit as a two-component spectrum to account for a small percentage of spatially isolated nitroxides present in the high-labeling stoichiometry sample. For any given set of parameters R, ξ, η, α, β, and γ the best fit to the data was obtained by linear least-squares minimization of the function

$$S(H_0) = c_1 S(H_0; R = 50\text{Å}, \xi = \eta = \alpha = \beta = \gamma = 0) + c_2 S(H_0; R, \xi, \eta, \alpha, \beta, \gamma) + c_3 \tag{12}$$

where the first term represents the spectrum of the spatially isolated component, the second term is the dipolar coupled component, and the third term is a constant baseline correction. As detailed previously (Hustedt et al., 1993), a search was performed to find the optimal x axis (δH_0) shift to best match the simulation with the data. A spline interpolation routine was used to directly overlay the shifted simulation onto the data. In the global analysis of the spectra obtained at X-, Q-, and W-band, no effort was made to keep the mol fractions of spatially isolated ($\chi_1 = c_1/[c_1 + c_2]$) and dipolar coupled ($\chi_2 = c_2/[c_1 + c_2]$) nitroxides equal for the three spectra. While all three spectra were obtained from the same sample preparation and were collected at approximately the same temperature, the spectra at different microwave frequencies were collected at different periods of time after sample preparation. As a result, minor variations in these mol fractions were not unexpected. The number of SL-NAD$^+$ bound per GAPDH tetramer is given by $4\chi_2$, assuming that a second SL-NAD$^+$ binds with equal probability to sites adjacent to and distant from the first (Beth et al., 1984). All calculations were performed on DEC 3000 400 or 200 4/233 alpha workstations (Digital Equipment Corporation, Maynard, MA). Anyone interested in obtaining computer programs used in this work should contact the authors.

Modeling based on known crystal structure

The chemical structure of N^6-SL-NAD$^+$ is shown in Fig. 2. Molecular modeling was performed using Insight II software (Biosym Technologies, San Diego, CA) running on a Silicon Graphics (Mountain Valley, CA) Indigo^2 workstation. The structure of the 6-membered ring nitroxide was constructed from the x-ray crystallographic data obtained by Berliner (1970) for 2,2,6,6-tetramethyl-4-piperidinol-1-oxyl. The atomic coordinates for a GAPDH dimer (red and green subunits of the tetramer) determined by Moras et al. (1975) for lobster muscle GAPDH were obtained from the Protein Data Bank (Brookhaven National Laboratory). The coordinates of the other two subunits (yellow and blue) were generated by rotation about the Q axis. In this structure, the pairs of R axis-related (red and green, yellow and blue) NAD$^+$ cofactors are in different conformations (*anti-syn*). This conformation is not consistent with the EPR data (Deparde et al., 1981; Beth et al., 1984) nor with subsequent x-ray crystallographic data obtained from human muscle GAPDH (Mercer et al., 1976). As previously described (Beth et al., 1984), the structure of the NAD$^+$ cofactors in the tetramer were adjusted such that all four had C_2 symmetry-related *anti* conformations.

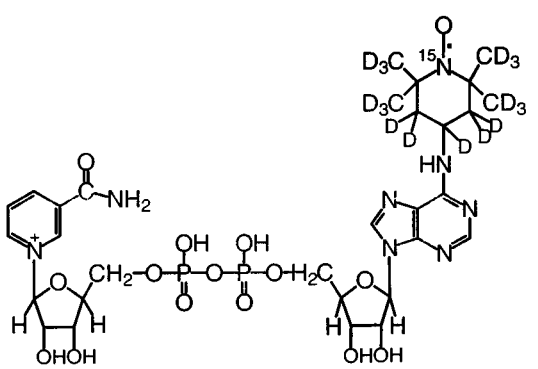

FIGURE 2 Structure of [^{15}N,D$_{17}$]-N^6-SL-NAD$^+$.

Bonds were created between the carbon atoms directly across from the nitroxide moiety of the spin-label and the amino groups on the adenine rings for each of the four subunits of the GAPDH tetramer. The torsion angles of the two bonds forming the C—N—C linkage between adenine and the spin-label were then adjusted to minimize the contact of the spin-label with adjacent side chains and to maximize the agreement of values of R (measuring from nitrogen to nitrogen), ξ, and η calculated for the model with those obtained from analysis of the EPR data. The torsion angles for all four subunits were adjusted equally to maintain the C_2 symmetry of the complex.

Calculation of EPR spectra of dipolar coupled nitroxides undergoing rigid body rotational diffusion

The EPR spectrum of a pair of dipolar coupled nitroxides undergoing rigid body isotropic rotational diffusion is calculated using a method based on the work of Robinson and co-workers (Robinson et al., 1992). The CW-EPR spectrum is obtained from the Fourier transform of a free induction decay (FID) time domain signal, which is calculated by solving the stochastic Liouville equation using a Monte Carlo approach to generate random molecular trajectories according to a Brownian isotropic rotational diffusion model.

Assuming the A- and g-tensors of the two nitroxides are equal and axial,

$$\begin{aligned} A^j_{xx} = A^j_{yy} = A_\perp \quad A^j_{zz} = A_\parallel \\ g^j_{xx} = g^j_{yy} = g_\perp \quad g^j_{zz} = g_\parallel \end{aligned} \tag{13}$$

and that $\xi = \eta = \alpha = \beta = \gamma = 0°$, the Hamiltonian may be written as

$$\begin{aligned} \hat{H} = {} & g'_{zz}\beta_e H_0(S^1_z + S^2_z) - \omega_n(I^1_z + I^2_z) \\ & + A'_{xz}(I^1_x S^1_z + I^2_x S^2_z) + A'_{zz}(I^1_z S^1_z + I^2_z S^2_z) \\ & - \frac{D}{4} S^1_+ S^2_- - \frac{D}{4} S^1_- S^2_+ + D S^1_z S^2_z \end{aligned} \tag{14}$$

where

$$\begin{aligned} A'_{xz} &= (A_\perp - A_\parallel)\cos\mu \sin\mu \\ A'_{zz} &= A_\perp \sin^2\mu + A_\parallel \cos^2\mu \\ g'_{zz} &= g_\perp \sin^2\mu + g_\parallel \cos^2\mu \end{aligned} \tag{15}$$

and for a ^{15}N nitroxide, $\omega_n = 1.54 \times 10^{-4} \times \omega_0$.

The classical isotropic rotational diffusion operator

$$\Gamma_\Omega = D_R \frac{1}{\sin\mu} \frac{\partial}{\partial\mu} \sin\mu \frac{\partial}{\partial\mu} \tag{16}$$

may be written in matrix form assuming an equally spaced grid of angles

$$\mu_i = \left(i - \frac{1}{2}\right)\Delta_\mu \quad \Delta_\mu = \frac{\pi}{N_\mu} \tag{17}$$

as derived by Robinson and co-workers (1992).

$$\Gamma_\Omega = \frac{D_R}{(\Delta_\mu)^2} M^{-1} T \tag{18}$$

where

$$M = \begin{pmatrix} \sin\mu_1 & 0 & 0 & \cdots \\ 0 & \sin\mu_2 & 0 & \cdots \\ \cdot & \cdot & \cdot & \cdot \\ \cdot & \cdot & 0 & \sin\mu_{N_\mu} \end{pmatrix} \tag{19}$$

and to achieve reflective boundary conditions.

$$T = \begin{pmatrix} \sin\mu_2 & -\sin\mu_2 & \cdot & \cdot & 0 \\ -\sin\mu_2 & (\sin\mu_2 + \sin\mu_3) & -\sin\mu_3 & \cdot & \cdot \\ \cdot & \cdot & \cdot & \cdot & \cdot \\ 0 & \cdot & \cdot & -\sin\mu_{N_\theta} & -\sin\mu_{N_\theta} \end{pmatrix} \tag{20}$$

Let $\dot{P}(t)$ be the vector giving the probability of being at each of the possible orientations, μ_j, at time t, and P_{eq} be the equilibrium distribution. The solution to

$$\dot{P}(t) = \Gamma_\Omega P(t) \tag{21}$$

is given by

$$P(t + \delta t) = e^{KM^{-1}T} P(t) \tag{22}$$

where $K = D_R\, \delta t/(\Delta_\mu)^2$ and $\Gamma_\Omega\, P_{eq} = 0$ for $(P_{eq})_j = 1/N_\mu$. In the limit of small K, Eq. 22 can be approximated by

$$P(t + \delta t) \approx (1 + KM^{-1}T)P(t) \tag{23}$$

The time increment Δt at which the FID must be calculated is determined by the Nyquist frequency of the Fourier transform and the desired width of the simulated spectrum. For $\Delta t = 2.5$ ns, the spectral width is ~140 Gauss (suitable for X- and Q-band) and for $\Delta t = 1.25$ ns the width is ~280 Gauss (suitable for W-band). To retain a linear equation similar in form to Eq. 23 and to obtain the desired spectral width, let $\Delta t = N_s \delta t$, then

$$\begin{aligned} P(t + \Delta t) &= e^{N_s KM^{-1}T} P(t) \\ &= (e^{KM^{-1}T})^{N_s} P(t) \\ &\approx (1 + KM^{-1}T)^{N_s} P(t) \end{aligned} \tag{24}$$

The matrix

$$F = (1 + KM^{-1}T\delta t)^{N_s} \tag{25}$$

has the property that

$$\sum_{j=1}^{j=N_\mu} F_{i,j} = 1 \tag{26}$$

The elements of the matrix G, defined as

$$G_{i,j} = \sum_{k=1}^{j} F_{i,k} \tag{27}$$

give the probability of rotating from orientation μ_j to orientation μ_i during the time interval Δt.

The FID in the rotating frame is generated by solving

$$S(\mu_0, t) = \mathrm{Tr}\{S_+ \rho(\mu_0, t)\} e^{-i\omega_0 t} \tag{28}$$

The density matrix, $\rho(\mu_0, t)$, is obtained by solving

$$\begin{aligned} \dot{\rho} = {} & -i[H(t), \rho(\mu_0, t)] \\ & - \Gamma_R(\rho(\mu_0, t) - \rho_{eq}) - \Gamma_\Omega(\rho(\mu_0, t) - \rho_{eq}) \end{aligned} \tag{29}$$

where Γ_R is a phenomenological relaxation rate operator. The treatment of the first two terms of Eq. 29 is described in detail in Appendix B.

Starting at time $t = 0$, let $\mu_0 = \mu_j$ and

$$\rho(\mu_0, t = 0) = \tfrac{1}{2}(S_+ + S_-) \tag{30}$$

Then,

$$\rho(\mu_0, t = \Delta t) = Q(\mu_j) \cdot \rho(\mu_0, t = 0) \cdot Q(\mu_j)^{-1} \tag{31}$$

After each time interval, Δt, a uniform random number, d, between 0 and 1 is chosen to determine the new orientation of the molecule. After the first time interval, the new orientation is $\mu(t + \Delta t) = \mu_k$ if $G_{k-1,j} < d \leq G_{k,j}$, so that

$$\rho(\mu_0, t = \Delta t) = Q(\mu_k) \cdot \rho(\mu_0, t = \Delta t) \cdot Q(\mu_k)^{-1} \tag{32}$$

and so on for each successive time interval.

Finally, the complete CW-EPR spectrum is obtained from the Fourier transform of $S(\mu_0, t)$ summed over all possible initial orientations and summed over a sufficient number of trajectories, N_{traj}, to give a smooth simulation.

$$S(\omega) = \frac{1}{N_{traj}} \int_0^\infty e^{-i\omega t} \left[\sum_{n=1}^{N_{traj}} \sum_{j=1}^{N_\mu} S(\mu_{0j}, t) P_{eq}(\mu_{0j}) \sin \mu_{0j} \right] dt \tag{33}$$

The expected rotational diffusion coefficient, D_R, and rotational correlation time, $\tau_c = 1/6\, D_R$, are given by

$$D_R = \frac{\pi^2 K N_s}{\Delta t (N_\mu)^2} \qquad \tau_c = \frac{\Delta t (N_\mu)^2}{6\pi^2 K N_s} \tag{34}$$

In addition to the calculation of the EPR spectrum from Eq. 33, the following autocorrelation functions are also calculated to evaluate whether the Monte Carlo method used is correctly modeling isotropic rotational diffusion.

$$\begin{aligned} C_1(t) &= \langle \cos \mu_0 \cos \mu(t) \rangle \\ C_2(t) &= \langle (1 - 3\cos^2\mu_0)(1 - 3\cos^2\mu(t)) \rangle \\ C_3(t) &= \langle (5\cos^3\mu_0 - 3\cos\mu_0)(5\cos^3\mu(t) - 3\cos\mu(t)) \rangle \end{aligned} \tag{35}$$

These correlation functions are expected to decay as single exponentials with decay times of $\tau_1 = 2D_R$, $\tau_2 = 6D_R$, and $\tau_3 = 12D_R$, respectively.

RESULTS

The EPR lineshape from two immobilized, dipolar coupled spin-labels will depend upon five independent angles and the distance between the unpaired electrons as defined in Fig. 1. Clearly, with this number of independent variables it is not possible to provide an exhaustive survey of the lineshapes that can be observed experimentally. However, it is possible to define the limits of sensitivity for measurement of interspin distances as a function of selected orientational models and as a function of microwave observer frequency. Figs. 3-5 show calculations performed at X-, Q- and W-band, respectively, assuming that the principal axes of the two spin-labels are coincident ($\alpha = \beta = \gamma = 0°$). Fig. 6 shows the effects of noncoincident axis frames.

Fig. 3 shows simulated X-band spectra for three selected orientational models. In the left column, the interelectron vector is parallel to the z axes of the two nitroxides ($\xi = 0°$). This represents the case of maximum sensitivity to R in the extrema regions (z-turning points) of the spectrum at X-band. From top to bottom, the simulations were performed for R = 50, 25, 20, 15, and 10 Å. At R = 25 Å (column 1, row 2), there are resolved splittings in the extrema regions of the spectrum with linewidths appropriate for perdeuterated nitroxide probes with measurable spectral broadening observed out to 30 Å (not shown). As R is decreased in the range from 25 to 10 Å, the spectral shapes clearly show the effect of increasing the magnitude of the principal element of the dipolar coupling tensor (column 1, rows 2–5). With this set of angles, interspin distances out to 30 Å can be characterized at X-band.

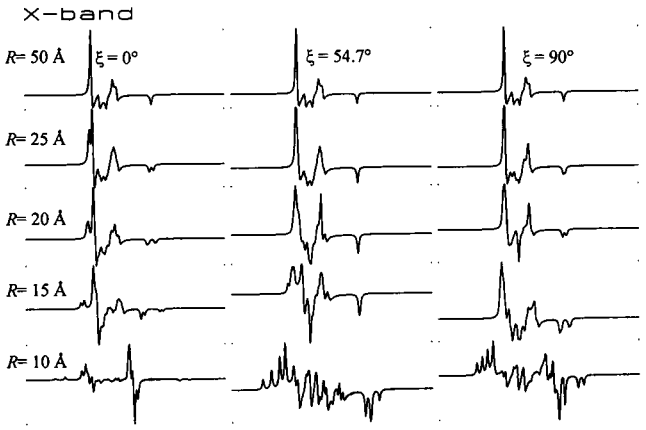

FIGURE 3 Simulated X-band CW-EPR spectra of dipolar coupled nitroxides. From left to right the three columns correspond to $\xi = 0°$, $\xi = 54.7°$, and $\xi = 90°$. From top to bottom R = 50, 25, 20, 15, and 10 Å. In all cases, $g_{xx} = 2.0085$, $g_{yy} = 2.0060$, $g_{zz} = 2.0020$; $A_{xx} = 10.0$ Gauss, $A_{yy} = 8.0$ Gauss, $A_{zz} = 45.0$ Gauss; $\eta = 0°$ and $\alpha = \beta = \gamma = 0°$; Lorentzian linewidth, $\Gamma = 0.75$ Gauss; 150 Gauss sweep width; $\omega_0 = 2\pi \cdot 9.8 \times 10^9\ s^{-1}$; H_{CF} =3500 Gauss.

Fig. 3, center column, shows simulated X-band spectra for the case where the z axes of each nitroxide are oriented at the magic angle ($\xi = 54.7°$) with respect to the interelectron vector. This represents the case of minimum sensitivity to R in the extrema regions of the spectrum at X-band. Even with this unfavorable geometry, there are distortions of spectral features in the center (x- and y-turning points) of the spectrum out to distances of 25 Å (column 2, row 2) with clearly resolved splittings at distances of 20 Å or less (column 2, rows 2–5).

Fig. 3, right column, shows simulated X-band spectra for the case where the z axes of each nitroxide are oriented orthogonal to the interelectron vector ($\xi = 90°$). This is a case of intermediate sensitivity to R in the extrema regions, but maximum sensitivity in the center of the spectrum at X-band. In this case, discernible broadening of interior spectral features are evident out to ~30 Å (not shown) with obvious splittings measurable by R = 25 Å (column 3, row 2). In the range from 25 to 10 Å, there is again a progressive increase in splitting of characteristic features throughout the

spectrum, which are indicative of both the relative spin-label geometry and the interelectron separation.

Fig. 4 shows simulations of the CW-EPR spectra at Q-band (ω_0 = 34 GHz) for the same three models as described for Fig. 3. At this frequency, the low-field end of the spectrum is determined by the magnitude of dipolar coupling along the x axes of the two nitroxides, while the high-field end of the spectrum is determined by the magnitude of dipolar coupling along the z axes. Two points are immediately obvious from the simulations at Q-band. First, the sensitivity to R is approximately equal to that described at X-band for each of the three orientational models considered. Second, the magnitude of dipolar coupling along the x- and y-nitroxide axes is much more clearly observable at the higher microwave frequency. Given the small sample sizes required for Q-band (2–3 μl) measurements on aqueous samples, the high signal-to-noise obtainable from modern Q-band instrumentation (Hyde et al., 1991), and the high orientational sensitivity of the spectral display, it is clear from these simulations that many systems exhibiting spin-spin coupling could be profitably studied at this microwave frequency (Eaton et al., 1980).

Fig. 5 shows simulations of the CW-EPR spectra at W-band (ω_0 = 94 GHz) for the same three models as described for Fig. 3. At this frequency, the spectral features from all nuclear hyperfine and dipolar coupling interactions along all three nitroxide principal axes are clearly resolved. While the sensitivity to interelectron separation is again comparable to that observed at X-band, the exquisite sensitivity to the magnitude of dipolar coupling along all three principal axes of the nitroxides provides a strong impetus for carrying out studies on systems at this higher frequency. The extremely small sample volumes required for W-band (70 nl) make this an attractive frequency for studies of spin-spin interactions when small sample volumes are an experimental constraint and when spin concentrations in the 100-μM range are attainable.

FIGURE 5 Simulated W-band CW-EPR spectra of dipolar coupled nitroxides. From left to right the three columns correspond to ξ = 0°, ξ = 54.7°, and ξ = 90°. From top to bottom R = 50, 25, 20, 15, and 10 Å. In all cases, g_{xx} = 2.0085, g_{yy} = 2.0060, g_{zz} = 2.0020; A_{xx} = 10.0 Gauss, A_{yy} = 8.0 Gauss, A_{zz} = 45.0 Gauss; η = 0° and α = β = γ = 0°; Lorentzian linewidth, Γ = 0.75 Gauss; 300 Gauss sweep width; ω_0 = $2\pi \cdot 94 \times 10^9$ s^{-1}; H_{CF} = 33510 Gauss.

Fig. 6 shows a panel of simulated spectra at X-, Q-, and W-band microwave frequencies for a constant interelectron separation of 15 Å. These simulations demonstrate the remarkable sensitivity of the lineshapes to the angles α, β, and γ (see figure legend for angles used), which determine the orientation of nitroxide 2 to nitroxide 1.

The EPR spectra of dipolar coupled nitroxides are sensitive to two distinct aspects of structure, the distance between the two nitroxides and the geometry relating them. In many applications, the relative orientation of the two probes can be as instructive as the distance, R. The simulations shown

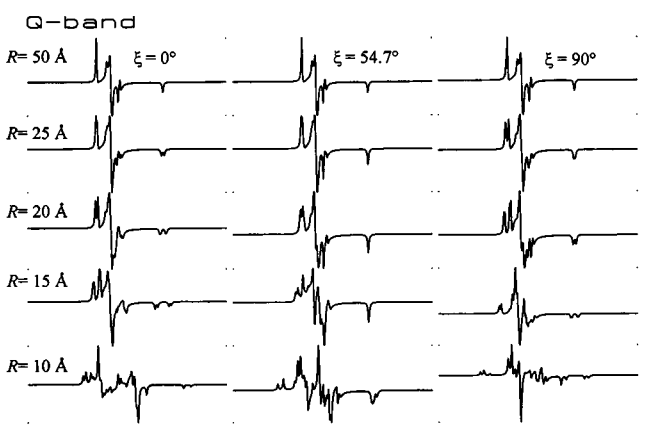

FIGURE 4 Simulated Q-band CW-EPR spectra of dipolar coupled nitroxides. From left to right the three columns correspond to ξ = 0°, ξ = 54.7°, and ξ = 90°. From top to bottom R = 50, 25, 20, 15, and 10 Å. In all cases, g_{xx} = 2.0085, g_{yy} = 2.0060, g_{zz} = 2.0020; A_{xx} = 10.0 Gauss, A_{yy} = 8.0 Gauss, A_{zz} = 45.0 Gauss; η = 0° and α = β = γ = 0°; Lorentzian linewidth, Γ = 0.75 Gauss; 200 Gauss sweep width; ω_0 = $2\pi \cdot 34 \times 10^9$ s^{-1}; H_{CF} = 12120 Gauss.

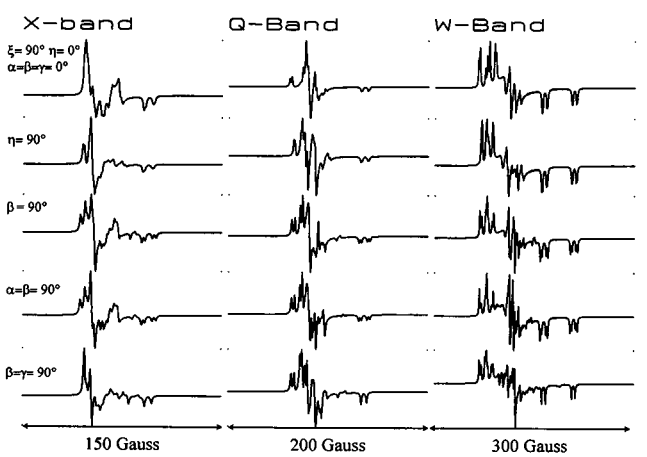

FIGURE 6 Effect of η, α, β, and γ on simulated CW-EPR spectra of dipolar coupled nitroxides. From left to right the three columns correspond to X-, Q-, and W-band simulations for ξ = 90°; R = 15 Å; η = 0° and α = β = γ = 0° (top row and others except as noted below); and all other parameters as described for Figs. 3–5. Second row from top, η = 90°. Third row, β = 90°. Fourth row, α = β = 90°. Fifth row, β = γ = 90°.

in Figs. 3–6 provide the motivation for development of a rigorous and computationally efficient method for the nonlinear least-squares analysis of data from dipolar coupled nitroxides in the rigid limit. Accurate determination of the distance and geometry between interacting spin-labels can provide important constraints for determining the structural elements of appropriately doubly labeled proteins.

Quantitative characterization of the dipolar coupling in N^6-SL-NAD^+-GAPDH

The CW-EPR spectra (*dots*) at X- and Q-band of N^6-SL-NAD^+ bound to microcrystalline, tetrameric GAPDH at low stoichiometry are shown in Fig. 7. The extraordinarily narrow linewidths evident in these spectra are indicative of a nitroxide probe which is tightly bound to GAPDH with very little, if any, local probe motion. Significant improvement in linewidth is also achieved by using a perdeuterated nitroxide label. These two spectra have been simultaneously fit (*solid lines*) to a powder pattern model. These fits give the A- and g-tensors that are necessary to analyze the EPR spectra of dipolar coupled nitroxides. It has been assumed, based on the symmetry of the crystal structure of the tetrameric NAD^+-GAPDH complex, that the A- and g-tensors are equivalent at the two sites. Given the excellent quality of the fits to the experimental data, this appears to be a valid assumption.

The CW-EPR spectra (dots) at X-, Q-, and W-band of N^6-SL-NAD^+ bound to microcrystalline, tetrameric GAPDH at high stoichiometry are shown in Fig. 8. The many additional splittings observed in these spectra, which are not evident in the spectra shown in Fig. 7, are a clear indication of dipolar coupling between nitroxides, in agreement with previous reports (Deparade et al., 1981; Beth et al., 1984). Two approaches have been used to analyze these spectra. The first approach is outlined in Table 1. From the splitting of the high-field features in these spectra, an estimate of R was obtained from Eq. 2 assuming that $\xi = 0°$ (16.1 Å) or $\xi = 90°$ (12.8 Å). Using these values as starting points, the three spectra were at first simultaneously analyzed allowing ξ, η, and R to vary. From these results it was clear that $\xi \approx 112°$ (or by symmetry 68°), $\eta \approx 118°$ (or by symmetry 62°), and $R \approx 13$ Å gave the best fit to the data. Next, the angle β was varied using $\beta = 45°$ and $\beta = 135°$ as initial values. Finally α, γ, and the linewidths of the dipolar coupled components were allowed to vary. At X- and Q-band the linewidth, Γ, of the spatially isolated component was fixed to that obtained from the analysis performed for Fig. 7, while the linewidth of the dipolar coupled component was allowed to vary. At W-band the linewidths of both components were allowed to vary, but were forced to be equal. No significant improvement in fit was obtained by allowing different linewidths for the spatially isolated and dipolar coupled components at W-band. As shown in

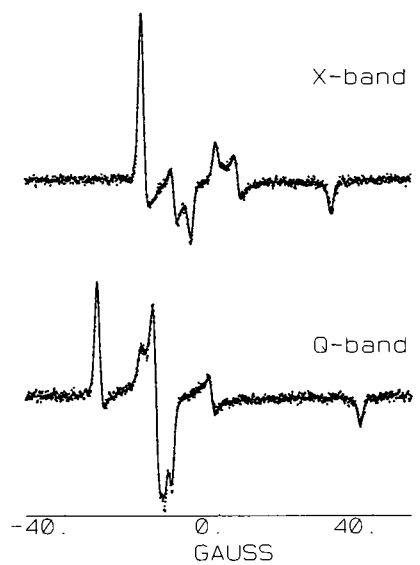

FIGURE 7 CW-EPR spectra (*dots*) at X- and Q-band of N^6-SL-NAD^+ bound to GAPDH at a ratio of 0.3 spin-labels per GAPDH tetramer. The two spectra have been simultaneously fit (*solid lines*) using previously described methods (Hustedt et al., 1993). The best fit parameters obtained are: $g' = 0.001599$, $g'' = 0.001459$, $\bar{g} = 2.0055$ (fixed), which gives $g_{xx} = 2.008558$, $g_{yy} = 2.005640$, $g_{zz} = 2.002302$; $A_{xx} = 10.804$ Gauss, $A_{yy} = 12.191$ Gauss, $A_{zz} = 49.008$ Gauss; Lorentzian linewidth, $\Gamma = 0.463$ Gauss; Gaussian convolution width, $\sigma = 0.470$ Gauss.

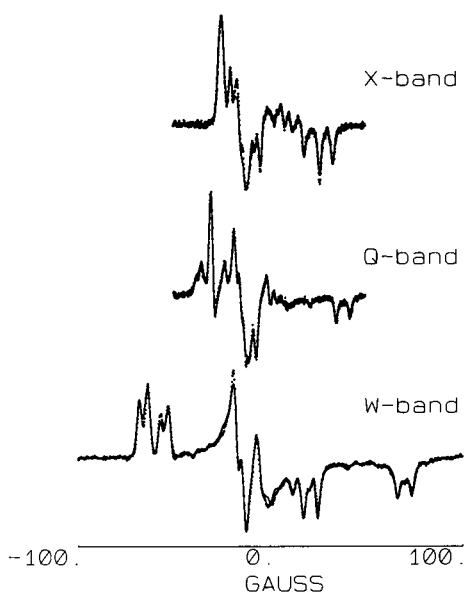

FIGURE 8 CW-EPR spectra (*dots*) at X-, Q-, and W-band of N^6-SL-NAD^+ bound to GAPDH at a ratio of 3.4 spin-labels per GAPDH tetramer. The simultaneous fits (*solid lines*) overlayed on the data were obtained as described in the text. The best-fit parameters obtained were: $\xi = 75.4°$, $\eta = 43.5°$, $R = 12.84$ Å, $\alpha = 161.1°$, $\beta = 53.5°$, and $\gamma = 19.0°$; the calculated labeling stoichiometry was 3.7 SL-NAD^+ per GAPDH tetramer at X-band, 3.7 at Q-band, and 3.4 at W-band; at X-band $\Gamma = 0.46$ Gauss (fixed) for the spatially isolated component and $\Gamma = 0.83$ Gauss for the dipolar coupled component; at Q-band $\Gamma = 0.46$ Gauss (fixed) for the spatially isolated component and $\Gamma = 0.68$ Gauss for the dipolar coupled component; at W-band $\Gamma = 1.27$ Gauss for both components; σ was fixed to 0.47 Gauss for all spectra.

TABLE 1 Results of the global analysis of the CW-EPR spectra of the N^6-SL-NAD^+-GAPDH complex at high labeling stoichiometry

	ξ	η	R	α	β	γ	Γ_X	Γ_Q	Γ_W	χ^2
Initial	0°	0°	16.1 Å	0°	0°	0°	0.463	0.463	0.463	169.0
Final	23°	—	17.6 Å	—	—	—	—	—	—	141.0
Initial	90°	0°	12.8 Å	0°	0°	0°	0.463	0.463	0.463	183.0
Final	93°	4°	12.9 Å	—	—	—	—	—	—	177.0
Initial	90°	60°	12.8 Å	0°	0°	0°	0.463	0.463	0.463	190.0
Final	112°	63°	13.0 Å	—	—	—	—	—	—	125.0
Initial	90°	120°	12.8 Å	0°	0°	0°	0.463	0.463	0.463	190.0
Final	112°	117°	13.0 Å	—	—	—	—	—	—	125.0
Initial	112°	63°	13.0 Å	0°	45°	0°	0.463	0.463	0.463	190.0
Final	106°	63°	15.0 Å	—	45°	—	—	—	—	159.0
Initial	112°	63°	13.0 Å	0°	135°	0°	0.463	0.463	0.463	153.0
Final	112°	45°	13.1 Å	—	135°	—	—	—	—	46.0
Initial	112°	117°	13.0 Å	0°	45°	0°	0.463	0.463	0.463	153.0
Final	112°	135°	13.1 Å	—	45°	—	—	—	—	46.0
Initial	112°	117°	13.0 Å	0°	135°	0°	0.463	0.463	0.463	189.0
Final	104°	117°	15.1 Å	—	135°	—	—	—	—	159.0
Initial	68°	63°	13.0 Å	0°	45°	0°	0.463	0.463	0.463	153.0
Final	68°	45°	13.1 Å	—	44°	—	—	—	—	46.0
Initial	68°	63°	13.0 Å	0°	135°	0°	0.463	0.463	0.463	190.0
Final	76°	63°	15.1 Å	—	135°	—	—	—	—	159.0
Initial	112°	45°	13.1 Å	0°	135°	0°	0.463	0.463	0.463	46.0
Final	105°	43°	12.84 Å	19°	126°	19°	0.68	0.83	1.25	7.26
Initial	112°	135°	13.1 Å	0°	45°	0°	0.463	0.463	0.463	46.0
Final	105°	137°	12.84 Å	19°	126°	−19°	0.68	0.83	1.25	7.26
Initial	68°	45°	13.1 Å	0°	44°	0°	0.463	0.463	0.463	46.0
Final	75°	43°	12.84 Å	−19°	54°	19°	0.68	0.83	1.25	7.26

The angles ξ, η, α, β, and γ, and the distance R, are defined in Fig. 1. The parameters Γ_X, Γ_Q, and Γ_W are the Lorentzian linewidths of the dipolar coupled component. At X- and Q-band, the linewidths of the spatially isolated component were fixed to those obtained in the analysis performed in Fig. 7. At W-band the linewidths of the spatially isolated and dipolar coupled components were made equal. Rows labeled "initial" give the input values used for the global analysis. Rows labeled "final" give the best-fit parameters obtained for these initial values; a dash indicates that the parameter was fixed to the initial value and was not varied. The χ^2 values were calculated as previously described (Beechem et al., 1991; Husted et al., 1993).

Table 1, three sets of angles were found that gave the same χ^2 for an interelectron distance of 12.84 Å. It is expected that a number of symmetry-related equivalent solutions should exist. The equivalence, by symmetry, of the three solutions in Table 1 is demonstrated by the fact that for all three solutions the values of R are equal; the values of χ^2 are equal; the angles ξ, η, and β are related by a reflection through 90°; and the angles α and γ are related by a reflection through 0°. These solutions are not distinguishable by EPR.

The second approach to the nonlinear least-squares analysis of the data in Fig. 8 is outlined in Table 2. Initially, the data at X-band alone were analyzed using a method based on simulated annealing. This generated 10 sets of parameters that could be used as starting points for the global analysis of all three spectra. Of 10 initial parameter sets, three produced fits that appeared to be at the same global minimum after ~10–30 iterations of the Marquardt-Levenberg algorithm. As with the stepwise approach, the distance and angles for the three best fits are equivalent (by symmetry). The agreement between the two approaches in the best-fit distance, angles, and χ^2 values strongly suggests that these values do in fact represent the global minimum in the χ^2 surface. The calculated values of the labeling stoichiometry obtained at the three different microwave frequencies are in reasonable agreement with the estimated value of 3.4 SL-NAD^+ bound per GAPDH tetramer.

Fig. 9 shows the confidence intervals for the six parameters relating nitroxide 1 to nitroxide 2, which were varied in the analysis shown in Fig. 8. In each panel, the x axis parameter was held fixed at certain values near the global minimum and the other five parameters were varied to find the best fit to the data. The horizontal lines are drawn at the χ^2 value corresponding to an approximate 99% confidence level calculated using the F-statistic. In some cases, such as R and ξ, the analysis of the X-band data alone (*open diamonds, dashed horizontal line*) is sufficient to precisely determine the best fit values. Little or no improvement is seen when the X- and Q-band data (*open circles, dotted horizontal line*) or the X-, Q-, and W-band data (*solid squares, solid horizontal line*) are simultaneously analyzed. On the other hand, significant improvement in the determination of η, α, β, and γ is seen when the higher frequency data are included. As expected, those angles requiring the resolution of x- and y-turning points of the spectra are most dramatically improved by including the higher frequency data.

TABLE 2 Results of the global analysis of the CW-EPR spectra of the N^6-SL-NAD$^+$-GAPDH complex at high labeling stoichiometry using initial values obtained from the simulated annealing fits to the X-band spectrum

	ξ	η	R	α	β	γ	Γ_X	Γ_Q	Γ_W	χ^2
Initial	73°	228°	12.8 Å	157°	56°	193°	1.06	1.06	1.06	11.2
X	75°	228°	12.8 Å	156°	56°	194°	0.80	—	—	7.8
X,Q,W	75°	223°	12.8 Å	161°	54°	199°	0.83	0.68	1.27	7.26
Initial	78°	143°	12.9 Å	194°	56°	156°	0.78	0.78	0.78	8.8
X	77°	143°	12.8 Å	194°	55°	156°	0.79	—	—	8.7
X,Q,W	75°	137°	12.8 Å	199°	54°	161°	0.83	0.68	1.27	7.26
Initial	109°	52°	13.2 Å	298°	49°	183°	1.03	1.03	1.03	27.0
X	106°	52°	13.0 Å	292°	51°	185°	0.99	—	—	23.0
Initial	75°	137°	12.8 Å	286°	55°	163°	1.06	1.06	1.06	23.4
X	74°	133°	12.8 Å	278°	55°	165°	0.99	—	—	21.1
Initial	78°	231°	13.0 Å	263°	50°	81°	1.19	1.19	1.19	25.5
X	75°	233°	12.8 Å	273°	50°	71°	1.20	—	—	33.4
Initial	104°	142°	12.9 Å	173°	54°	97°	1.18	1.18	1.18	23.1
X	103°	142°	12.8 Å	171°	53°	97°	0.98	—	—	20.4
Initial	105°	228°	12.9 Å	203°	125°	193°	1.20	1.20	1.20	14.4
X	105°	228°	12.8 Å	204°	124°	194°	0.80	—	—	7.8
X,Q,W	105°	223°	12.8 Å	199°	126°	199°	0.83	0.68	1.23	7.26
Initial	105°	132°	12.8 Å	156°	166°	124°	0.90	0.90	0.90	71.1
X	104°	146°	12.8 Å	177°	141°	127°	1.03	—	—	44.0
Initial	103°	144°	12.9 Å	167°	155°	125°	1.17	1.17	1.17	54.9
X	146°	104°	12.8 Å	177°	142°	126°	1.04	—	—	44.0
Initial	77°	142°	12.8 Å	194°	157°	56°	0.82	0.82	—	53.9
X	75°	130°	12.8 Å	197°	127°	108°	1.05	—	—	23.2

All parameters used are defined for Table 1. Rows labeled "X" are the results of analysis of the X-band data alone; Rows labeled "X,Q,W" are the results of the simultaneous analysis of the X-, Q-, and W-band spectra. When results at X-, Q-, and W-band are not given, the χ^2 values obtained were greater than 20.

Molecular modeling of N^6-SL-NAD$^+$-GAPDH complex

Fig. 10 shows the structure of the N^6-SL-NAD$^+$-GAPDH tetrameric complex generated as described above. Simultaneous adjustment of the torsion angles of the C—N and N—C bonds linking the NAD$^+$ to the spin-label moiety resulted in a structure with a measured distance between spin-labels (nitrogen to nitrogen) of R = 12.85 Å, and angles $\xi = 76°$, $\eta = 59°$, $\alpha = 253°$, $\beta = 36°$, and $\gamma = 289°$. In this orientation the nitroxides are free of any significant steric interaction with adjacent side chains of the protein and reasonable agreement with the EPR data is obtained for the distance, R, and the angles, ξ, η, and β.

Effect of global isotropic rotational diffusion on the CW-EPR spectra of dipolar coupled nitroxides

Figs. 11 and 12 show simulations of the CW-EPR spectra at X-, Q-, and W-band of a pair of dipolar coupled nitroxides undergoing isotropic rotational diffusion assuming axially symmetric A- and g-tensors and $\xi = \eta = \alpha = \beta = \gamma = 0°$, for R = 50 Å (Fig. 11) or R = 15 Å (Fig. 12). In each case, the top row is a rigid limit calculation ($D = 0$ or $\tau_c = \infty$). The other calculations show EPR spectra calculated for rotational correlation times that are within the sensitivity range of linear EPR spectroscopy of nitroxide spin-labels (τ_c = 125 ns, τ_c = 20 ns, and τ_c = 5 ns). These calculations demonstrate that, as expected, global rotational diffusion alters the lineshapes produced by dipolar coupled nitroxides. However, it is not until the rotational diffusion rate is sufficiently fast (τ_c = 5 ns) to average the anisotropic A-, g-, and D-tensors that the additional splittings produced by the dipolar interactions are lost.

Calculations (*dashed lines*) based on the rigid limit formalism of Eq. 10 are overlaid on the spectra on the top row of Figs. 11 and 12 (calculated for $\tau_c = \infty$). Calculations (*dashed lines*) performed using the algorithms developed by Freed and co-workers (Schneider and Freed, 1989) for spatially isolated nitroxides are overlaid on the spectra in Fig. 11, left-hand column, bottom three rows. For R = 50 Å, there is negligible dipolar coupling and the calculated spec-

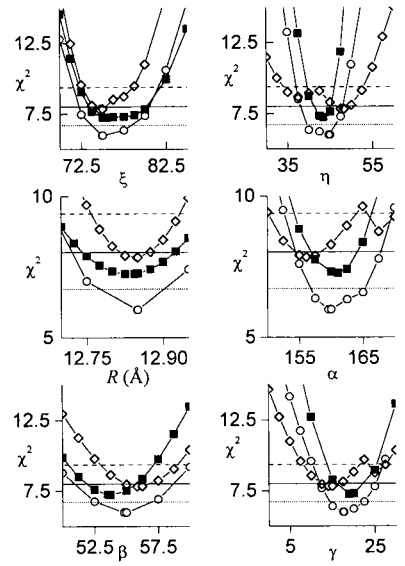

FIGURE 9 χ^2 surfaces for the fitting parameters ξ, η, R, α, β, and γ. The symbols used are as follows: (◇) fit to X-band data alone; (○) simultaneous fit to X- and Q-band data; (■) simultaneous fits to X-, Q-, and W-band data. The horizontal lines define ~99% confidence levels for each of the parameters for the (- - -) fit to X-band data alone; (····) fit to X- and Q-band data; (——) fit to X-, Q-, and W-band data.

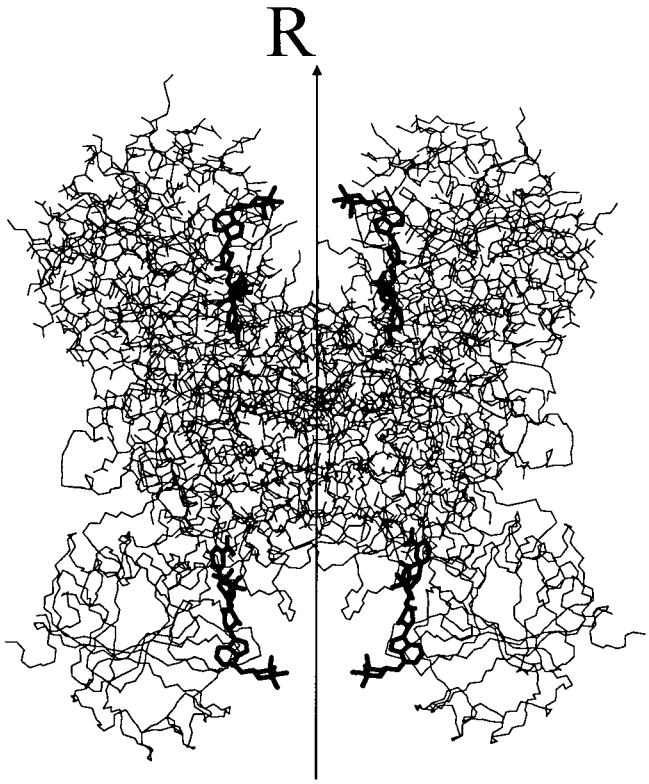

FIGURE 10 Structure of N^6-SL-NAD^+-GAPDH tetramer as determined from the molecular modeling. All four N^6-SL-NAD^+ cofactors are shown in bold. The lower pair of GAPD subunits shows the backbone only. The upper pair shows backbone and side chains. The crystallographic R axis is extending upward through the tetramer.

tra should be similar to those obtained using the algorithms of Freed and co-workers. All of the overlaid spectra agree well with the simulations generated using the molecular trajectory approach of Eq. 33. The overlays on the top rows of Figs. 11 and 12 demonstrate that the two methods (Eq. 10 and 33) produce nearly identical results in the rigid limit. Specifically, the assumptions made leading to Eq. 10, setting $\omega_n = 0$ and neglecting transitions allowed by mixing of nuclear spin states, are reasonable under these conditions. The overlays on the bottom three rows of the left-hand column of Fig. 11 demonstrate that the molecular trajectory approach gives results in close agreement with those obtained by using algorithms developed by Freed and co-workers (Schneider and Freed, 1989) for spatially isolated nitroxides.

For the calculation shown in the lower left-hand corner of Fig. 11, the following parameters were used,

$$\Delta t = 2.5 \times 10^{-9} \text{ second} \quad N_\mu = 128$$

$$N_s = 1000 \quad N_{traj} = 256 \quad K = 0.13835$$

which give expected values of $D_R = 33.3 \times 10^{-6}\ s^{-1}$, $\tau_1 = 15$ ns, $\tau_2 = 5$ ns, and $\tau_3 = 2.5$ ns. Excellent fits to the calculated correlation functions (data and fits not shown) were obtained using single exponential decays with actual best fit decay times of $\tau_1 = 15.5$ ns, $\tau_2 = 4.95$ ns, and $\tau_3 = 2.48$ ns. Remarkably, the molecular trajectory approach outlined above is a reasonable model for isotropic rotational diffusion, even when $N_s > N_\mu$.

DISCUSSION

Historically, the use of EPR spectroscopy of dipolar coupled nitroxide spin-labels to determine structural features of proteins and other macromolecular systems has been limited by the paucity of systems that intrinsically contain appropriate sites for spin-labeling. However, advances in the techniques of molecular biology now provide the ability to introduce specific labeling sites into target proteins. By judicious selection of sites for introduction of cysteine residues, nitroxides can be selectively incorporated into proteins in close enough proximity to produce measurable dipolar coupling (Hubbell et al., 1996). These advances in site-directed spin-labeling have prompted the development of the methods reported in this work, which can be used to rigorously analyze data from these new experiments.

Mechanisms of spin-spin coupling

Determination of the distance between interacting spin-labels requires consideration of two different mechanisms of interaction. The first, exchange coupling, is often a close range effect, which in the simplest form requires overlap of the molecular orbitals containing the unpaired electrons either from static proximity or by collisions due to dynamic

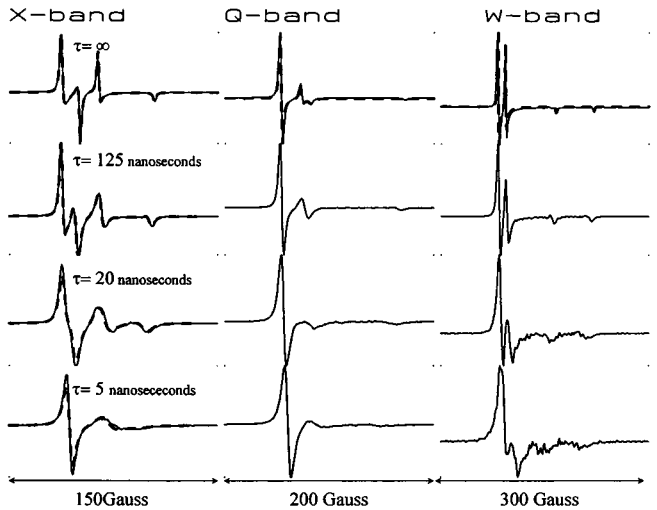

FIGURE 11 Simulations of the CW-EPR spectra at X-, Q-, and W-band of dipolar coupled nitroxides undergoing rigid body isotropic rotational diffusion with $\xi = \eta = \alpha = \beta = \gamma = 0°$ and $R = 50$ Å; $g_\perp = 2.00725$; $g_\parallel = 2.00200$; $A_\perp = 9.0$ Gauss; $A_\parallel = 45.0$ Gauss. The isotropic rotational correlation times, $\tau_c = 1/6D$, are from top to bottom: $\tau_c = \infty$, $\tau_c = 125$ ns, $\tau_c = 20$ ns, $\tau_c = 5$ ns. $T_{2e} = 76$ ns, corresponding to a linewidth of 0.75 Gauss. Field and frequency parameters were the same as used for Figs. 3–6. Overlaid on the top row are simulations (*dashed lines*) calculated using the rigid limit model of Eq. 10. Overlaid on the bottom three rows of the left-hand column are simulations (*dashed lines*) calculated using the algorithms of Schneider and Freed (1989) for spatially isolated nitroxides.

processes. The second, dipolar coupling, is a longer range effect, which arises from magnetic interactions between the unpaired electrons. A comprehensive review of these two

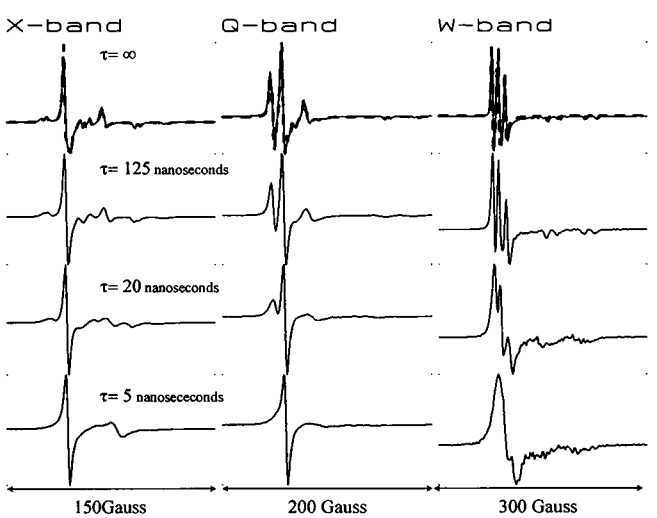

FIGURE 12 Simulations of the CW-EPR spectra at X-, Q-, and W-band of dipolar coupled nitroxides undergoing rigid body isotropic rotational diffusion with $\xi = \eta = \alpha = \beta = \gamma = 0°$ and $R = 15$ Å; $g_\perp = 2.00725$; $g_\parallel = 2.00200$; $A_\perp = 9.0$ Gauss; $A_\parallel = 45.0$ Gauss. The isotropic rotational correlation times, $\tau_c = 1/6D$, are from top to bottom: $\tau_c = \infty$, $\tau_c = 125$ ns, $\tau_c = 20$ ns, $\tau_c = 5$ ns. $T_{2e} = 76$ ns. Field and frequency parameters were the same as used for Figs. 3–6. Overlaid on the top row are simulations (*dashed lines*) calculated using the rigid limit model of Eq. 10.

mechanisms of spin-spin coupling has been provided by Eaton and Eaton (1989). The interested reader is directed to this review, and references therein, for an in-depth discussion of the area. In the range of 10–30 Å, dipolar coupling between nitroxide spin-labels often dominates the experimental EPR spectrum for large macromolecules that exhibit rotational correlation times in the slow motion regime ($\tau_c >$ 100 ns). Given that dipole-dipole interactions produce characteristic spectral effects, the important question becomes how to analyze these spectral effects in terms of accurate structural models. Early work showed that it is possible to obtain an estimate of the distance, R, between two nitroxides from the apparent magnitude of D, the unique element of the dipolar coupling tensor (see Luckhurst, 1976), which can be approximated from the splitting of characteristic spectral features (Jost and Griffith, 1972). The relatively weak cube-root dependence of R on the magnitude of D somewhat minimizes problems of obtaining a reasonable estimate of D from simple inspection of the EPR spectrum. However, the results in Figs. 3–6 demonstrate that the lineshape effects of dipolar coupling depend critically upon the distance between the two interacting spins and the five unique angles that specify the orientation of the principal axes of the two nitroxides (Fig. 1). Clearly, the EPR spectrum contains two separate pieces of structural information, the radial distance of separation between the two nitroxides and their relative orientations, both of which can provide direct insight into the structure of the macromolecule to which the spin-labels are attached.

Sensitivity of CW-EPR spectra to dipolar coupling between nitroxide spin-labels

As shown in Figs. 3–6, dipole-dipole interactions produce distinct effects in the EPR spectra at all three microwave frequencies in the absence of rotational diffusion. The spectral effects of the dipolar coupling along all three spin-label principal axes are clearly enhanced at the higher microwave frequencies. In this regard, the high resolution of spectral features at W-band at all three turning points of both spectral manifolds is particularly impressive, as shown in Figs. 5 and 6 (right column). For most orientational models, there are obvious spectral distortions due to dipole-dipole interactions out to distances approaching 30 Å. Even in the worst case, where both nitroxide z axes are oriented at the magic angle with respect to the interelectron vector using X-band EPR, there are measurable spectral distortions at separations of 25 Å (Fig. 3, center column) with linewidths appropriate for perdeuterated spin-labels. Unlike fluorescence resonance energy transfer, where transfer efficiency vanishes ($\kappa^2 = 0$) at certain orientations of the donor and acceptor dipoles, the intrinsic three-dimensional character of the nitroxide A- and g-tensors guarantees that there is no orientation of the two probes where the effects of dipolar coupling on the lineshape will vanish. In general, the magnitude of dipolar coupling can be observed in an experimental

CW-EPR spectrum if the splitting it produces is comparable to, or larger than, the widths of relevant spectral features. For this reason, perdeuterated spin-labels have been used in this work to reduce the extent of inhomogeneous broadening of spectral features, thereby enabling resolution of smaller dipolar couplings than would be possible using normal isotope spin-labels (Beth et al., 1984; Park and Trommer, 1989). As a general guide, perdeuteration of the nitroxide ring reduces the width of the low field line from ~4.5 Gauss to 2 Gauss in the rigid limit at X-band microwave frequency (Beth et al., 1981). Eq. 2 indicates that a 2-Gauss dipolar coupling ($2D$) will be observed at ~30 Å and that a 4.5-Gauss coupling ($2D$) will be observed at ~23 Å. This simple calculation provides a reasonable indication of the maximum distances that can be observed in the CW-EPR spectrum using normal isotope and perdeuterated spin-labels in the absence of other spectral broadening effects.

In the present work, ^{15}N has been used in place of ^{14}N in the spin-label moiety to reduce the computation time for nonlinear least-squares fitting of the data as described in Materials and Methods. It should be emphasized, however, that comparable sensitivity to dipolar coupling is provided by perdeuterated ^{14}N spin-labels as discussed in previous work (Beth et al., 1984).

Analysis of CW-EPR data from dipolar coupled spin-labels in the rigid limit

The determination of the distance of separation and relative orientation of two interacting spin-labels starts with the spin Hamiltonian of Eq. 1 (Eaton and Eaton, 1989). In the present work, a computationally efficient algorithm has been developed based upon this spin Hamiltonian, as described in Materials and Methods. This algorithm has been incorporated into an automated nonlinear least-squares spectral fitting routine based upon the Marquardt-Levenberg method (Hustedt et al., 1993). Previously, the program MENO originally developed by Eaton and co-workers (Eaton et al., 1983) for the analysis of metal-nitroxide interactions had been used to analyze the EPR spectra obtained from GAPDH labeled with N^6-SL-NAD^+ (Beth et al., 1984). This previous work showed that the observed EPR spectrum was reasonably consistent with the distance and geometry predicted from a molecular model derived from the known crystal structure of the GAPDH tetramer. However, the quality of the fits indicated that not all of the spectral features could be accounted for based solely on parameters obtained from the molecular model. With the computer resources available at that time, it was not practical to systematically explore more refined fitting of the experimental EPR data due to the number of degrees of freedom of the problem (i.e., five angles and a distance). In the present work, the EPR data from the N^6-SL-NAD^+-GAPDH complex have been reevaluated by combining an algorithm specifically developed for the efficient calculation of the EPR spectra of dipolar coupled nitroxides, the power of modern computational resources, and the ability to carry out global nonlinear least-squares fitting of multiple data sets to optimize agreement between computed and experimental spectra. This effort was undertaken to determine if a unique solution to the multidimensional dipolar coupling problem could be obtained from this well-defined system without the aid of a molecular model to guide initial values for the six independent variables. In addition, we wished to explore the utility of multifrequency EPR data in assuring a unique fit of the experimental data.

Due to the complicated nature of the dipolar interaction as illustrated in Fig. 1, there are many local minima in the χ^2 error surface for fitting the experimental data from dipolar coupled spin-labels. Initializing the global analysis algorithm with random initial values for all six parameters routinely led to unacceptable fits of the experimental spectra in Fig. 8 and to recovery of different parameters for different initial values. The complex nature of the χ^2 surface is further illustrated by the fact that when the results from previous molecular modeling work (Beth et al., 1984) were used as initial values, unacceptable fits were also obtained. However, two independent approaches have been found that provided accurate fitting of the experimental data as shown in the overlays in Fig. 8. First, instead of allowing all six of the parameters to be varied at each iteration of the Marquardt-Levenberg routine, the fitting was carried out stepwise as described in Table 1. This approach yielded a much improved fit of the data as compared to that obtained using the parameters from the molecular model in previous work (Beth et al., 1984). While successful in this particular case, the step-wise approach did not appear to be one that would be generally, and easily, applicable to other systems. As a result, a second method was developed which, it was hoped, would require less operator intervention and would provide a general method for finding the global χ^2 minimum.

In this second approach, the global χ^2 surface was explored using the method of simulated annealing (Press et al., 1992) as described in Materials and Methods. Simulated annealing is well-suited to problems of this type since it is not prone to being trapped in local minima before the error surface has been thoroughly explored. As shown in Table 2, the simulated annealing approach yielded several sets of parameters that yielded relatively low χ^2 values. When these sets of parameters were used to initiate the Marquardt-Levenberg routine, three of the sets led to fits with the same χ^2, and recovery of the same angles and distance as was obtained using the stepwise approach. The excellent agreement of the computed and experimental spectra at all three microwave frequencies strongly suggests that these represent the global minimum of the error surface.

The applicability of the simulated annealing approach was further examined by analyzing calculated EPR spectra (with added random noise) for different orientational models exhibiting resolved dipolar coupling. In the three separate models tested, this approach permitted recovery of the simulation parameters (data not shown). Based upon these

results and those obtained for GAPDH, it appears that EPR data from dipolar coupled spin-labels can be rigorously analyzed without any initial knowledge of the distance and geometry relating the two probes in systems where the probes are static and have a well-defined relative geometry, leading to highly resolved spectral features. It should be emphasized that even though the current studies were carried out on ammonium sulfate-precipitated N^6-SL-NAD^+-GAPDH complex where global rotational diffusion is absent, the same highly resolved dipolar splittings were observed in the EPR spectrum of the enzyme in solution where the rotational correlation time is >100 ns (Beth et al., 1984). In this work, polycrystalline enzyme was used for two reasons. First, the N^6-SL-NAD^+ unbound at equilibrium can be removed by washing, lessening the total number of spectral components to be fit (although the unbound component could have been easily incorporated into the linear least-squares step of Eq. 12). Secondly, the use of multiple microwave frequencies required that the samples be stored for variable periods of time between individual measurements and the samples are much more stable in the precipitated form. In general, it should be possible to analyze CW-EPR spectra of dipolar coupled nitroxides using the approach developed here as long as the rotational correlation time is longer than or near the rigid limit (i.e., $\tau_c > 100$ ns).

Advantages of multiple microwave frequency characterization of dipolar coupled nitroxide spin-labels

The χ^2 surfaces for the six fitting parameters shown in Fig. 9 demonstrate that the parameters α, γ, and η are better defined from the simultaneous fits of the experimental data at X- and Q-bands and at X-, Q-, and W-bands than they are at X-band alone. This is to be expected since the interior of the spectrum at X-band is complicated by overlap of lines from both nuclear manifolds in the presence of dipolar coupling. It could be argued, based upon the current data alone, that the gains from higher frequency measurements, and from combined analyses of multifrequency measurements, are modest. However, this may not be true in most systems. The dipolar coupling from N^6-SL-NAD^+ bound to GAPDH is an idealized case where the two spin-labels are related by C_2 symmetry, the binding sites are equivalent, and hence the nitroxides exhibit the same *A*- and *g*-tensors, and the interelectron distance is relatively small, leading to large spectral shifts due to the dipolar coupling. All of these factors contribute to the comparatively sharp minima in the χ^2 plots shown in Fig. 9. Simple inspection of the calculated spectra shown in Figs. 3–6 indicates that the increased resolution of spectral features along all three principal axes of the nitroxides leads to better observation of the orientation of the reference frame of the D-tensor in the reference frames of the two nitroxides. This increased resolution should contribute in a substantial way to determining the values for the various fitting parameters in those systems where the two spin-labels are not bound in identical sites and not related by C_2 symmetry. Indeed, this will be the case in most applications of the site-directed spin-labeling method and many other systems as well.

Molecular model of the N^6-SL-NAD^+-GAPDH complex using the derived distance and geometry constraints

By using the distance and geometry information obtained from fitting the experimental EPR data in Fig. 8, a molecular model of the complex has been constructed as shown in Fig. 10. In constructing this model, the position of all atoms of NAD^+ were left in the same position as determined from the crystal structure of the enzyme (Moras et al., 1975), after correcting the crystal structure to have an *anti* conformation for all of the bound NAD^+ subunits (Beth et al., 1984), and the spin-label moiety was positioned relative to the adenine ring by rotations about the C—N—C bonds. Obviously, there are many assumptions inherent in constructing such a model, including the positioning of the NAD^+ backbone, the six-membered ring conformation of the nitroxide moiety, and the differences in primary structure between lobster and rabbit muscle GAPDH, to cite a few. Therefore, the important point of this model is not that it is correct at the level of positioning of individual atoms, but rather that the parameters determined from fitting the EPR data are very reasonable given the dimensions and steric constraints of the coenzyme binding pockets of the GAPDH tetramer.

Alternative approaches to determining inter-spin-label distances

Recently, Rabenstein and Shin (1995) have developed a Fourier deconvolution method for determining electron-electron distances from CW-EPR spectra of dipolar coupled nitroxides and applied their method to a series of doubly spin-labeled α-helical peptides in the frozen state. This method assumes that the nitroxides are rotationally immobile on the linear EPR time-scale and that the two nitroxides are oriented randomly (isotropically) with respect to each other due to the flexibility of the peptide and the tethers attaching the nitroxides to the peptide. In this latter aspect, the Fourier deconvolution method represents the opposite extreme of the case considered in this work, where the nitroxides are assumed to be held in a fixed orientation relative to one another.

A number of different time-domain EPR techniques have also been developed as methods for measuring electron spin-spin distances in the frozen state, including the "2+1" electron spin echo method (Raitsimring et al., 1992), the double electron-electron resonance (DEER) spin echo method (Pfannebecker et al., 1996; Larsen and Singel, 1993), the measurement of T_{1e} and T_{2e} by saturation recovery EPR (SR-EPR) and electron spin echo (ESE) methods (Rakowsky et al., 1995), and a double quantum 2-dimen-

sional Fourier transform EPR method (Saxena and Freed, 1996). For all of these methods, the potential exists for measuring distances significantly >30 Å, since the upper limit on distance measurement is not determined by the inhomogeneous linewidth as it is for CW-EPR. For example, Raitsimring et al. (1992) determined the distance distribution between a pair of spin-labels in tetrameric hemoglobin to be a function centered at 35 Å with a half-width of 3 Å. Typically, however, these time domain techniques have been used to measure distances in the 10–20 Å range in model or biological systems.

Rakowsky et al. (1995) have found that metal-nitroxide distance measurements in spin-labeled low-spin iron porphyrins using CW-EPR, ESE measurements of T_{2e}, and SR-EPR measurements of T_{1e}, all give consistent results. In many systems, the combined use of CW and time domain methods, when applicable, will likely prove to be very valuable.

Effects of dynamics on dipolar coupled spin-labels

It is clear that each of the methods for determining interprobe distances from dipolar coupled spin-labels reported to date, including the present work, is applicable to a subset of systems of contemporary interest. It is important to begin to develop analytical methods for determining molecular distances between spin-labels for molecules in liquid solution where one, or both, of the nitroxides are not rotationally immobile or where the relative orientation between the two nitroxides is neither completely random nor rigidly fixed. The simulations presented in Figs. 11 and 12 are an initial step in this direction. A similar problem occurs in the analysis of fluorescence resonance energy transfer data in terms of an interprobe (donor and acceptor) distance distribution when there is motion of the two probes relative to each other. van der Meer and co-workers (1993) have shown that it is possible to treat this problem in terms of discrete set of orientational states with dynamics driving transitions between states.

There are two approaches that can be developed for the modeling of dipolar coupled nitroxides undergoing rotational dynamics. The first is the extension of the molecular trajectory approach used here to more complex dynamic models involving motion of the nitroxides relative to one another. Steinhoff and Hubbell (1996) have recently calculated EPR spectra by modeling side-chain dynamics of a (singly) spin-labeled polyleucine trimer using Brownian dynamics trajectories. The second approach is the application of methods developed by Freed and co-workers (Schneider and Freed, 1989) for the rapid solution of the stochastic Liouville equation for a variety of dynamic models to the case of dipolar coupled spin-labels. Both of these approaches will be used in the future development of methods, which will allow for the analysis of CW-EPR spectra of doubly labeled biomolecules in terms of the local and global dynamics of the nitroxides and the internitroxide geometry. The choice of which approach to use will depend on the experimental system and the particular dynamic model to be tested.

APPENDIX A

For spatially isolated nitroxides at X-band, the nuclear Zeeman term produces relatively small (<0.2 Gauss) shifts in the eigenvalues of the Hamiltonian and significantly smaller shifts in the resonant positions of the allowed transitions ($\delta_{m_I,m_I'} = 0$). Assuming that the nuclear Zeeman terms have similar negligible effects on the CW-EPR spectra of dipolar coupled nitroxides greatly simplifies the diagonalization of the Hamiltonian in Eq. 1. Setting $\omega_n = 0$, the following transformations are applied to the Hamiltonian.

$$\hat{H}' = U_2 U_1 \hat{H} U_1^{-1} U_2^{-1} \tag{A1}$$

$$U_1 = e^{-\epsilon^1 I_z^1} e^{-\epsilon^2 I_z^2} \quad U_2 = e^{-\zeta^1 I_y^1} e^{-\zeta^2 I_y^2} \tag{A2}$$

The effect of the transformation U_2 is to mix states $|m_S^1 m_S^2 m_I^1 m_I^2\rangle$ with those of the form $|m_S^1 m_S^2 m_{I\pm1}^1 m_{I\pm1}^2\rangle$. The result is non-zero transition probabilities

$$P_{\Psi\to\Psi'} = |\langle\Psi|S_+^1 + S_+^2|\Psi'\rangle|^2 \tag{A3}$$

for the "forbidden" transitions $\delta_{m_I^1,m_I^{1'}} \neq 0$ and $\delta_{m_I^2,m_I^{2'}} \neq 0$. In the case of spatially isolated nitroxides at X-band, these transition probabilities are quite small (<0.001) and can be safely ignored. Neglecting the mixed states produced by U_2 and continuing to use the product basis as the eigenbasis, H' can be written in terms of four 4 × 4 blocks along the diagonal for a pair of ^{15}N nitroxides and nine such blocks for a pair of ^{14}N nitroxides.

The 4 × 4 blocks of $\hat{H}'$ are given by

$$\hat{H}^{k'} = \begin{pmatrix} pH_0 + c^k + D/4 & 0 & 0 & 0 \\ 0 & qH_0 + f^k - D/4 & -D/4 & 0 \\ 0 & -D/4 & -qH_0 - f^k - D/4 & 0 \\ 0 & 0 & 0 & -pH_0 - c^k + D/4 \end{pmatrix} \tag{A4}$$

where the basis states are given by

$$\Psi^k = \begin{pmatrix} |m_s^1 = +\tfrac{1}{2} m_s^2 = +\tfrac{1}{2} m_I^1 m_I^2\rangle \\ |m_I^1 = +\tfrac{1}{2} m_s^2 = -\tfrac{1}{2} m_I^1 m_I^2\rangle \\ |m_s^1 = -\tfrac{1}{2} m_s^2 = +\tfrac{1}{2} m_I^1 m_I^2\rangle \\ |m_s^1 = -\tfrac{1}{2} m_s^2 = -\tfrac{1}{2} m_I^1 m_I^1\rangle \end{pmatrix} \tag{A5}$$

where

$$p = \frac{\beta_e}{2}(g_{zz}^1 + g_{zz}^2) \quad q = \frac{\beta_e}{2}(g_{zz}^1 - g_{zz}^2)$$

$$c^k = \frac{\gamma_e}{2}(A_{eff}^1 m_I^1 + A_{eff}^2 m_I^2) \tag{A6}$$

$$f^k = \frac{\gamma_e}{2}(A_{eff}^1 m_I^1 - A_{eff}^2 m_I^2)$$

The eigenvalues are

$$\begin{aligned} \lambda_1^k &= pH_0 + c^k + D/4 \\ \lambda_2^k &= \sqrt{(D/4)^2 + (qH_0 + f^k)^2} - D/4 \\ \lambda_3^k &= -\sqrt{(D/4)^2 + (qH_0 + f^k)^2} - D/4 \\ \lambda_4^k &= -pH_0 - c^k + D/4 \end{aligned} \tag{A7}$$

with eigenvectors

$$|\Psi_1^k\rangle = \begin{pmatrix} 1 \\ 0 \\ 0 \\ 0 \end{pmatrix} \quad |\Psi_2^k\rangle = \begin{pmatrix} 0 \\ \nu_1^k \\ -\nu_2^k \\ 0 \end{pmatrix} \tag{A8}$$

$$|\Psi_3^k\rangle = \begin{pmatrix} 0 \\ \nu_2^k \\ \nu_1^k \\ 0 \end{pmatrix} \quad |\Psi_4^k\rangle = \begin{pmatrix} 0 \\ 0 \\ 0 \\ 1 \end{pmatrix}$$

where the (unnormalized) values of ν_1^k and ν_2^k are given by

$$\nu_1^k \propto qH_0 + f^k + \sqrt{(D/4)^2 + (qH_0 + f^k)^2}$$

$$\nu_2^k \propto D/4 \tag{A9}$$

APPENDIX B

At each value of $\mu = \mu_j$, for a pair of ^{15}N nitroxides, the full 16 × 16 Hamiltonian of Eq. 14 is defined numerically. Let

$$V_1 = \begin{pmatrix} 1 & 0 & 0 & 0 \\ 0 & \nu_1' & \nu_1' & 0 \\ 0 & \nu_1'' & -\nu_1'' & 0 \\ 0 & 0 & 0 & 1 \end{pmatrix} \tag{B1}$$

where each of the elements of V_1 in Eq. B1 is a 4 × 4 block and

$$\nu_1' = \frac{1}{\sqrt{2}} \begin{pmatrix} 1 & 0 & 0 & 0 \\ 0 & 1 & 0 & 0 \\ 0 & 0 & 1 & 0 \\ 0 & 0 & 0 & 1 \end{pmatrix} \quad \nu_1'' = \begin{pmatrix} 1 & 0 & 0 & 0 \\ 0 & 0 & 1 & 0 \\ 0 & 1 & 0 & 0 \\ 0 & 0 & 0 & 1 \end{pmatrix} \tag{B2}$$

then $H'(\mu_j) = V_1^{-1} \cdot H(\mu_j) \cdot V_1$ is block (4 × 4) diagonal. The eigenvalues and eigenvectors of each of the four 4 × 4 blocks are found numerically using standard routines (Press et al., 1992). The full set of eigenvalues, λ_i, and eigenvectors, $(V_2)_i$, is then used to generate a solution to

$$\dot{\rho} = -i[H(\mu_j), \rho(t)] \tag{B3}$$

Let

$$\Lambda_{i,j} = e^{-i\lambda_i \Delta t} \delta_{i,j} \quad V = V_1 \cdot V_2 \quad Q(\mu_j) = V \cdot \Lambda \cdot V^{-1} \tag{B4}$$

then,

$$\rho(t + \Delta t) = Q(\mu_j) \cdot \rho(t) \cdot Q^{-1}(\mu_j) \tag{B5}$$

To account for the effects of Γ_R all elements of $\rho(\mu, t + \Delta t)$ that are not within the four 4 × 4 blocks along the diagonal are multiplied by $e^{-\Delta t/t_{2e}}$ after each time interval Δt, where T_{2e} is the intrinsic electron spin-spin relaxation time. It should be noted that rotational modulation of the nonsecular terms of the dipolar Hamiltonian, which are not included in this treatment, could in principle produce linewidth effects that are not included in these calculations.

The authors wish to thank Dr. Marcia Newcomer for assistance with the molecular modeling, Dr. David Piston for providing access to the Silicon Graphics workstation, Scott M. Blackman for assistance in interpreting the molecular model and for constructive comments on the manuscript, and Dr. Wieb van der Meer for reviewing the manuscript before submission.

This work was supported in part by National Institutes of Health Grants HL 34737, RR 04075, and RR 01811.

REFERENCES

Altenbach, C., T. Marti, H. Gobind Khorana, and W. L. Hubbell. 1990. Transmembrane protein structure: spin labeling of bacteriorhodopsin mutants. *Science.* 248:1088–1092.

Beechem, J. M., E. Gratton, M. Ameloot, J. R. Knutson, and L. Brand. 1991. The global analysis of fluorescence intensity and anisotropy decay data: second generation theory and programs. *In* Topics in Fluorescence Spectroscopy, Vol. 2: Principles. J. R. Lakowicz, editor. Plenum Press, New York. 241–305.

Berliner, L. J. 1970. Refinement and location of the hydrogen atoms in the nitroxide 2,2,6,6-tetramethyl-4-piperidinol-1-oxyl. *Acta Crystallogr. B.* B26:1198–1202.

Beth, A. H., K. Balasubramanian, B. H. Robinson, L. R. Dalton, S. D. Venkataramu, and J. H. Park. 1983. Sensitivity of V_2' saturation transfer electron paramagnetic resonance signals to anisotropic rotational diffusion with [^{15}N] nitroxide spin labels. Effects of noncoincident magnetic and diffusion tensor principal axes. *J. Phys. Chem.* 87:359–367.

Beth, A. H., B. H. Robinson, C. E. Cobb, L. R. Dalton, W. E. Trommer, J. J. Birktoft, and J. H. Park. 1984. Interactions and spatial arrangement of spin-labeled NAD^+ bound to glyceraldehyde-3-phosphate dehydrogenase: comparison of EPR and X-ray modeling data. *J. Biol. Chem.* 259:9717–9728.

Beth, A. H., S. D. Venkataramu, K. Balasubramanian, L. R. Dalton, B. H. Robinson, D. E. Pearson, C. R. Park, and J. H. Park. 1981. ^{15}N- and ^{2}H-substituted maleimide spin-labels: improved sensitivity and resolution for biological EPR studies. *Proc. Natl. Acad. Sci. U.S.A.* 78: 967–971.

Dalton, L. R. 1985. EPR and Advanced EPR Studies of Biological Systems. CRC Press, Boca Raton, FL. 314 pp.

Deparade, M. P., K. Glöggler, and W. E. Trommer. 1981. Isolation and characterization of glyceraldehyde-3-phosphate dehydrogenase from a sturgeon from the Caspian sea and its interaction with spin-labeled NAD^+ derivatives. *Biochim. Biophys. Acta.* 659:422–433.

Eaton, S. S., and G. R. Eaton. 1989. Resolved electron-electron spin-spin splittings in EPR spectra. *In* Biological Magnetic Resonance, Vol. 8: Spin Labeling Theory and Applications, L. J. Berliner and J. Reuben, editors. Plenum Press, New York. 340–398.

Eaton, S. S., K. M. More, D. L. DuBois, P. M. Boymel, and G. R. Eaton. 1980. Metal-nitroxyl interactions. 15. Comparison of EPR spectra at X band and Q band. *J. Magn. Reson.* 41:150–157.

Eaton, S. S., K. M. More, B. M. Sawant, P. M. Boymel, and G. R. Eaton. 1983. Metal-nitroxyl interactions. 29. EPR studies of spin-labeled copper complexes in frozen solution. *J. Magn. Reson.* 52:435–449.

Farahbakhsh, Z. T., K. D. Ridge, H. G. Khorana, and W. L. Hubbell. 1995. Mapping light-dependent structural changes in the cytoplasmic loop connecting helices C and D in rhodopsin: a site-directed spin labeling study. *Biochemistry.* 34:8812–8819.

Freed, J. 1976. Theory of slow tumbling ESR spectra for nitroxides. *In* Spin Labeling: Theory and Applications. L. J. Berliner, editor. Academic Press, New York. 53–132.

Hanson, P., G. Martinez, G. Millhauser, F. Formaggio, M. Crisma, C. Toniolo, and C. Vita. 1996a. Distinguishing helix conformations in alanine-rich peptides using the unnatural amino acid TOAC and electron spin resonance. *J. Am. Chem. Soc.* 118:271–272.

Hanson, P., G. Millhauser, F. Formaggio, M. Crisma, and C. Toniolo. 1996b. ESR characterization of hexameric, helical peptides using double TOAC spin labeling. *J. Am. Chem. Soc.* 118:7618–7625.

Hubbell, W. L., and C. Altenbach. 1994. Site-directed spin labeling of membrane proteins. *In* Membrane Protein Structure: Experimental Approaches. S. H. White, editor. Oxford University Press, New York. 224–248.

Hubbell, W. L., H. S. Mchaourab, C. Altenbach, and M. A. Lietzow. 1996. Watching proteins move using site-directed spin labeling. *Structure.* 4:779–783.

Hustedt, E. J., C. E. Cobb, A. H. Beth, and J. M. Beechem. 1993. Measurement of rotational dynamics by the simultaneous nonlinear analysis of optical and EPR data. *Biophys. J.* 64:614–621.

Hyde, J. S., M. E. Newton, R. A. Strangeway, J. G Camenisch, and W. Froncisz. 1991. *Rev. Sci. Instrum.* 32:2969–2975.

Jost, P., and O. H. Griffith. 1972. Electron spin resonance and the spin labeling method. *In* Methods in Pharmacology, Vol. 2. C. F. Chignell, editor. Appleton-Century-Crofts, New York. 223–276.

Larsen, R. G., and D. J. Singel. 1993. Double electron-electron resonance spin-echo modulation: spectroscopic measurement of electron spin pair separations in orientationally disordered solids. *J. Chem. Phys.* 98: 5134–5146.

Liu, J., J. M. Rutz, P. E. Klebba, and J. B. Feix. 1994. A site-directed spin-labeling study of ligand induced conformational changes in the ferric enterobactin receptor, Fep A. *Biochemistry.* 33:13274–13283.

Luckhurst, G. R. 1976. Biradicals as spin probes. *In* Spin Labeling: Theory and Applications. L. J. Berliner, editor. Academic Press, New York. 133–181.

Mchaourab, H. S., M. A. Lietzow, K. Hideg, and W. L. Hubbell. 1996. Motion of spin-labeled side chains in T4 lysozyme. correlation with protein structure and dynamics. *Biochemistry.* 35:7692–7704.

Mercer, W. D., S. I. Winn, and H. C. Watson. 1976. Twinning in crystals of human skeletal muscle D-glyceraldehyde-3-phosphate dehydrogenase. *J. Mol. Biol.* 104:277–283.

Miick, S. M., G. V. Martinez, W. R. Fiori, A. P. Todd, and G. L. Millhauser. 1992. Short alanine based peptides may form 3_{10}-helices, and not α-helices in aqueous solution. *Nature.* 359:653–655.

Millhauser, G. L. 1992. Selective placement of electron spin resonance spin labels: new structural methods for proteins and peptides. *Trends in Biochem. Sci.* 17:448–452.

Moras, D., K. W. Olsen, M. N. Sabesan, M. Buehner, G. C. Ford, and M. G. Rossmann. 1975. Studies of asymmetry in the three-dimensional structure of lobster D-glyceraldehyde-3-phosphate dehydrogenase. *J. Biol. Chem.* 250:9137–9162.

Oh, K. J., H. Zhan, C. Cui, K. Hideg, R. J. Collier, and W. L. Hubbell. 1996. Organization of diphtheria toxin T domain in bilayers: a site-directed spin labeling study. *Science.* 273:810–812.

Park, J. H., and W. E. Trommer. 1989. Advantages of ^{15}N and deuterium spin probes for biomedical electron paramagnetic resonance investigations. *In* Biological Magnetic Resonance, Vol. 8: Spin Labeling Theory and Applications. L. J. Berliner and J. Reuben, editors. Plenum Press, New York. 547–595.

Pfannebecker, V., H. Klos, M. Hubrich, T. Volkmer, A. Heuer, U. Wiesner, and H. W. Spiess. 1996. Determination of end-to-end distances in oligomers by pulsed EPR. *J. Phys. Chem.* 100:13428–13432.

Press, W. H., S. A. Teukolsky, W. T. Vetterling, and B. P. Flannery. 1992. Numerical Recipes in FORTRAN: The Art of Scientific Computing. Cambridge University Press, New York. 963 pp.

Rabenstein, M. D., and Y.-K. Shin. 1995. Determination of the distance between two spin labels attached to a macromolecule. *Proc. Natl. Acad. Sci. U.S.A.* 92:8239–8243.

Raitsimring, A., J. Peisach, H. C. Lee, and X. Chen. 1992. Measurement of distance distribution between spin labels in spin-labeled hemoglobin using an electron spin echo method. *J. Phys. Chem.* 96:3526–3531.

Rakowsky, M. H., K. M. More, A. V. Kulikov, G. R. Eaton, and S. S. Eaton. 1995. Time-domain electron paramagnetic resonance as a probe of electron-electron spin-spin interaction in spin-labeled low-spin iron porphyrins. *J. Am. Chem. Soc.* 117:2049–2057.

Robinson, B. H., L. Slutsky, and F. Auteri. 1992. Direct simulation of continuous wave electron paramagnetic resonance spectra from Brownian dynamics trajectories. *J. Chem. Phys.* 96:2609–2616.

Saxena, S., and J. H. Freed. 1996. Double quantum two-dimensional Fourier transform electron spin resonance: distance measurements. *Chem. Phys. Lett.* 251:102–110.

Schneider, D. J., and J. H. Freed. 1989. Calculating slow motional magnetic resonance spectra: a user's guide. *In* Biological Magnetic Resonance, Vol. 8: Spin Labeling Theory and Applications. L. J. Berliner and J. Reuben, editors. Plenum Press, New York. 1–76.

Shin, Y.-K., C. Levinthal, F. Levinthal, and W. L. Hubbell. 1993. Colicin E1 binding to membranes: time-resolved studies of spin labeled mutants. *Science.* 259:960–963.

Smirnov, A. I., T. I. Smirnova, and P. D. Morse II. 1995. Very high frequency electron paramagnetic resonance of 2,2,6,6-tetramethyl-1-piperidinyloxy in 1,2-dipalmitoyl-*sn*-glycero-3-phosphatidylcholine liposomes: partitioning and molecular dynamics. *Biophys. J.* 68: 2350–2360.

Steinhoff, H.-J., and W. L. Hubbell. 1996. Calculation of electron paramagnetic resonance spectra from Brownian dynamics trajectories: application to nitroxide side chains in proteins. *Biophys. J.* 71:2201–2212.

van der Meer, B. W., M. A. Raymer, S. L. Wagoner, R. L. Hackney, J. M. Beechem, and E. Gratton. 1993. Designing matrix models for fluorescence energy transfer between moving donors and acceptors. *Biophys. J.* 64:1243–1263.

Voss, J., M. M. He, W. L. Hubbell, and H. R. Kaback. 1996. Site-directed spin labeling demonstrates that transmembrane domain XII in the lactose permease of *Escherichia coli* is an α-helix. *Biochemistry.* 35: 12915–12918.

Voss, J., L. Salwinski, H. R. Kabach, and W. L. Hubbell. 1995a. A method for distance determination in proteins using a designed metal ion binding site and site-directed spin labeling: evaluation with T4 lysozyme. *Proc. Natl. Acad. Sci. U.S.A.* 92:12295–12299.

Voss, J., W. L. Hubbell, and H. R. Kabach. 1995b. Distance determination in proteins using designed metal ion binding sites and site-directed spin labeling: application to the lactose permease of *Escherichia coli. Proc. Natl. Acad. Sci. U.S.A.* 92:12300–12304.

Wang, W., R. L. Belford, R. B. Clarkson, P. H. Davis, J. Forrer, M. J. Nilges, M. D. Timken, T. Walczak, M. C. Thurnauer, J. R. Norris, A. L. Morris, and Y. Zwang. 1994. Very high frequency EPR-94 GHz instrument and applications to primary reaction centers from photosynthetic red bacteria and to other disordered systems. *Appl. Magn. Reson.* 6:195–215.